

## Property- and Structure-Guided Discovery of a Tetrahydroindazole Series of Interleukin-2 Inducible T-Cell Kinase Inhibitors

Jason D. Burch,<sup>\*,†</sup> Kevin Lau,<sup>†</sup> John J. Barker,<sup>‡</sup> Fred Brookfield,<sup>‡</sup> Yong Chen,<sup>||</sup> Yuan Chen,<sup>†</sup> Charles Eigenbrot,<sup>†</sup> Claire Ellebrandt,<sup>§</sup> M. Hicham A. Ismaili,<sup>†</sup> Adam Johnson,<sup>†</sup> Daniel Kordt,<sup>§</sup> Colin H. MacKinnon,<sup>‡</sup> Paul A. McEwan,<sup>‡</sup> Daniel F. Ortwine,<sup>†</sup> Daniel B. Stein,<sup>§</sup> Xiaolu Wang,<sup>§</sup> Dirk Winkler,<sup>§</sup> Po-Wai Yuen,<sup>||</sup> Yamin Zhang,<sup>||</sup> Ali A. Zarrin,<sup>†</sup> and Zhonghua Pei<sup>†</sup>

<sup>†</sup>Genentech Inc., 1 DNA Way, South San Francisco, California 94080, United States

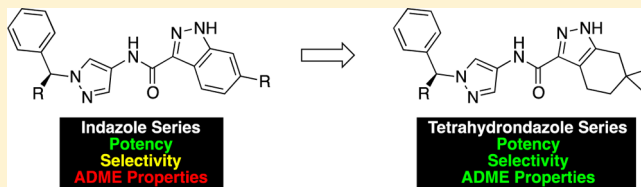
<sup>‡</sup>Evotec (U.K.) Ltd., 114 Milton Park, Abingdon, Oxfordshire OX14 4SA, United Kingdom

<sup>§</sup>Manfred Eigen Campus, Evotec AG, Essener Bogen 7, D-22419, Hamburg, Germany

<sup>||</sup>Pharmaron Beijing Co. Ltd., No. 6 Tai He Road, BDA, 100176, Beijing, China

### S Supporting Information

**ABSTRACT:** Interleukin-2 inducible T-cell kinase (ITK), a member of the Tec family of tyrosine kinases, plays a major role in T-cell signaling downstream of the T-cell receptor (TCR), and considerable efforts have been directed toward discovery of ITK-selective inhibitors as potential treatments of inflammatory disorders such as asthma. Using a previously disclosed indazole series of inhibitors as a starting point, and using X-ray crystallography and solubility forecast index (SFI) as guides, we evolved a series of tetrahydroindazole inhibitors with improved potency, selectivity, and pharmaceutical properties. Highlights include identification of a selectivity pocket above the ligand plane, and identification of appropriate lipophilic substituents to occupy this space. This effort culminated in identification of a potent and selective ITK inhibitor (GNE-9822) with good ADME properties in preclinical species.



## INTRODUCTION

IL-2 inducible T cell kinase (ITK) is a nonreceptor tyrosine kinase belonging to the Tec family of kinases involved in T cell development, differentiation, and effector function.<sup>1</sup> Tec family kinases include ITK, resting lymphocyte kinase (RLK), Bruton's tyrosine kinase (Btk), tyrosine kinase expressed in hepatocellular carcinoma (Tec), and bone marrow expressed kinase (Bmx). Except for Bmx, which is expressed in endothelial cells, the Tec kinases are primarily expressed in hematopoietic cells.<sup>1</sup> T cells express ITK, RLK, and Tec, however, analyses of knockout mice have established a prominent role for ITK and RLK as two critical Tec kinases that integrate T cell receptor signaling (TCR) to activate phospholipase C gamma-1 (PLC $\gamma$ 1) and subsequently Ca<sup>2+</sup> mobilization.<sup>2</sup> Several groups have shown that ITK deficiency results in defective T helper 2 (T<sub>H</sub>2) cell function.<sup>3</sup> Specifically, in ITK<sup>-/-</sup> mice lung inflammation, eosinophil infiltration and mucous production are drastically reduced in response to challenge with ovalbumin.<sup>4</sup>

Prompted by the wealth of preclinical evidence supporting the role of ITK in allergic asthma and other inflammatory disorders, intense pharmaceutical research has been directed toward development of selective inhibitors of this kinase.<sup>5</sup> Furthermore, preclinical in vivo activity using ITK inhibitors has been achieved, resulting in the reduction of IL-2 production in one example<sup>5f</sup> and the reduction of IL-4 production and lung inflammation in another.<sup>5b</sup>

We have recently disclosed the discovery of an indazole series of ITK inhibitors, which evolved from the moderately potent and selective HTS hit **1** into the exceptionally potent inhibitor **3** (Figure 1).<sup>5m,6</sup> While the potency and selectivity of indazole **3** compare favorably with previous inhibitors disclosed in the literature, this series in general required improvement of ADME properties such as solubility and permeability. We attributed the solubility to high aromatic ring count (4–5) and moderate lipophilicity (cLogD<sub>7.4</sub> ~ 2–3), while the suboptimal permeability could be attributed to the relatively high topological polar surface area (TPSA, typically >120) and H-bond donor count (3) for our best molecules. Guided by structure- and property-based optimization techniques, we sought to improve both of these characteristics simultaneously in a second round of optimization, which led to the discovery of a saturated subseries: the “tetrahydroindazole” or THI series.

## CHEMISTRY

Two reaction sequences with divergent regiochemical consequences were imperative to our construction of tetrahydroindazole carboxylates **6**, **8**, and **10** (Scheme 1). For THIs possessing substitution at the C<sub>5</sub> position (**8iv** and **10**), a Claisen condensation between ketones **4iv** or **9<sup>7</sup>** and diethyl

Received: April 8, 2014

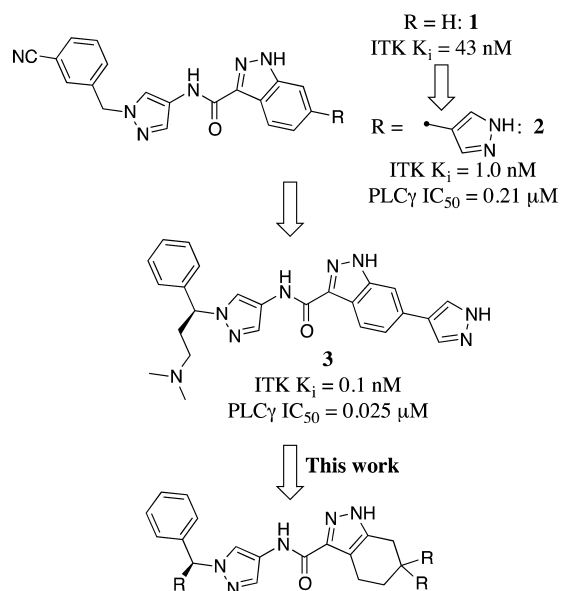
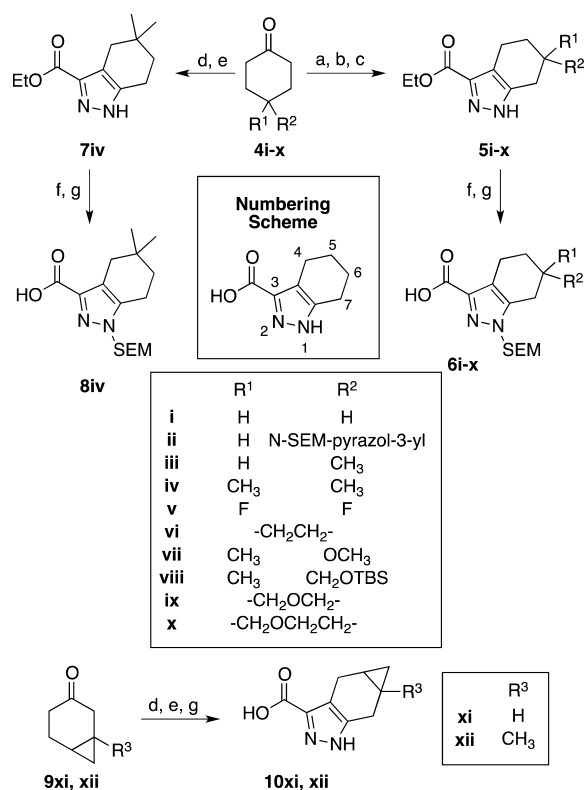


Figure 1. Evolution of the indazole series of ITK inhibitors.

### Scheme 1. Synthesis of Tetrahydroindazole Carboxylic Acids **6**, **8**, and **10**<sup>a</sup>



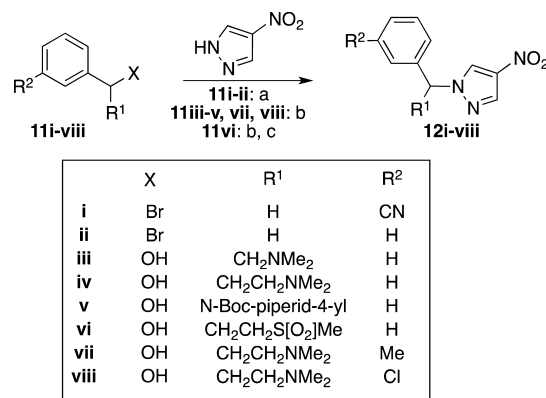
<sup>a</sup>Reagents and conditions: (a) ethyl diazoacetate, LDA, THF,  $-78$  °C; (b) POCl<sub>3</sub>, pyr, rt; (c) *n*-octane, 110 °C; (d) diethyl oxylate, NaOEt, EtOH, rt; (e) hydrazine, AcOH, rt; (f) SEM-Cl, NaH, THF, 0 °C  $\rightarrow$  rt; (g) LiOH, THF/ACN/H<sub>2</sub>O, rt.

oxylate,<sup>8</sup> followed by ring closure with hydrazine, provided the desired ethyl pyrazolyl carboxylates. SEM protection and ester hydrolysis of **7iv** provided the requisite protected acid **8iv**, whereas pyrazole carboxylic acids **10** were obtained without SEM protection, as we subsequently determined protection of the pyrazole NH was unnecessary. In general, however, we were

more interested in THIs possessing C<sub>6</sub> substitution (vide infra), and thus we required an alternative approach to convert symmetric ketones **4** to the desired tetrahydroindazole carboxylates **6**. We were drawn to a rarely utilized transformation disclosed by Padwa and co-workers in which pyrazole carboxylic esters were formed by addition of the lithium anion of ethyl diazoacetate to ketones, followed by dehydration and thermal cycloisomerization.<sup>9</sup> Although, to the best of our knowledge, the only cyclic ketone to which this reaction had been applied prior to our work was cyclohexanone, we realized that mechanistically this reaction would specifically afford the alternative regioisomer relative to the Claisen chemistry, starting with the same ketone **4**.<sup>10</sup> We successfully applied this methodology to a diverse set of 4-substituted cyclohexanones **4**, providing ethyl pyrazolyl carboxylates **5i-x**, which were subsequently converted to the protected acids **6i-x** as above.

Formation of the western fragments **12** was straightforward and followed chemistry disclosed previously for the indazole series (Scheme 2).<sup>5sm</sup> 3-nitropyrazole can either be directly

### Scheme 2. Synthesis of Benzylated Nitropyrazoles **12**<sup>a</sup>



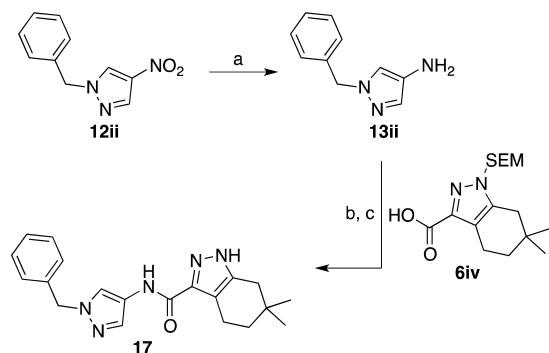
<sup>a</sup>Reagents and conditions: (a) K<sub>2</sub>CO<sub>3</sub>, DMF, rt; (b) PPh<sub>3</sub>, DEAD, THF, 0 °C  $\rightarrow$  rt; (c) mCPBA, CH<sub>2</sub>Cl<sub>2</sub>, rt.

benzylated with benzyl bromides and sodium hydride, or secondary benzylic alcohols can be merged with 3-nitropyrazole using Mitsunobu conditions.<sup>11</sup> For nitropyrazole **12vi** containing a sulfone appendage, the Mitsunobu reaction was done at the sulfide oxidation state, and a subsequent mCPBA-mediated oxidation afforded the sulfone.

Completion of the synthesis of our target inhibitors is exemplified by the endgame toward representative inhibitor **17** (Scheme 3). Hydrogenative reduction of nitropyrazole **12ii** yielded aminopyrazole **13ii**, which was then immediately acylated without purification with THI carboxylic acid **6iv** using TBTU. Deprotection using an aqueous acid/aqueous base protocol provided the target inhibitor **17**. The additional aqueous base operation is necessary to remove residual *N*-hydroxymethyl pyrazole byproducts that remain in varying quantities following SEM deprotection. For inhibitors possessing stereogenic elements, racemic mixtures were resolved into single isomers by supercritical fluid chromatography on chiral stationary phases at the final stage.

## RESULTS AND DISCUSSION

The ITK active site, represented by the X-ray cocrystal structure with inhibitor **2** (Figure 2),<sup>5sm</sup> contains four residues

Scheme 3. Representative Completion of Inhibitor 17<sup>a</sup>

<sup>a</sup>Reagents and conditions: (a) H<sub>2</sub> (1 atm), 10% Pd/C, EtOH, rt; (b) 6i, TBTU, <sup>i</sup>Pr<sub>2</sub>NEt, DMF, rt; (c) HCl in dioxane, 60 °C; NaOH(aq), EtOH, rt.

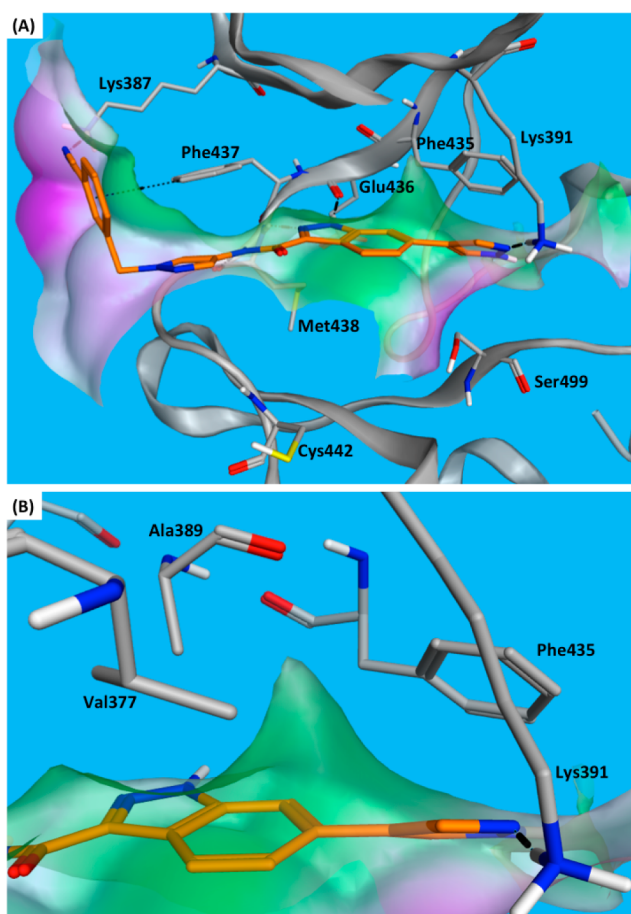


**Figure 2.** (A) Co-crystal structure of 2 with the kinase domain of ITK.<sup>5m</sup> Protein–ligand hydrogen bonds and  $\pi$ – $\pi$  stacking interactions are denoted by dashed lines with cylinders. The solvent accessible surface of the protein is color coded by lipophilic potential (pink is polar, green is hydrophobic).<sup>13</sup> (B) Close-up view of ITK selectivity pocket (vide infra).

which distinguish it from other kinases: two phenylalanine residues (the “gatekeeper” Phe435 and Phe437), a cysteine residue (Cys442), and a serine residue (Ser499). The phenylalanine pair alone is fairly unique, with only 14 of >450 kinases possessing this combination, and neither the Phe/Phe/Cys nor the Phe/Phe/Ser triad are contained in any other kinase in the kinome.<sup>12</sup> For the indazole class of ITK inhibitors,

four polar and two nonpolar interactions contribute to the binding efficiency of these inhibitors. A tridentate array of hydrogen bonds with the hinge region (carbonyl of Glu436; carbonyl and NH of Met438) and a hydrogen bond between the pyrazole NH and the side chain of Lys391 account for the polar interactions. An edge-to-face  $\pi$ -stacking interaction between the ligand phenyl group and Phe437 and face-to-face  $\pi$ -stacking between the ligand pyrazole and Phe435 are also important. The latter Phe435 interaction coupled with the Lys391 hydrogen bond is postulated to account for the 40-fold potency improvement between 1 and 2 (ITK  $K_i$  43 nM  $\rightarrow$  1.0 nM); the additional 10-fold potency increase between 2 and 3 (ITK  $K_i$  1.0 nM  $\rightarrow$  0.1 nM) can be rationalized by reduction of the rotational degrees of freedom which results through introduction of the benzylic stereocenter, thereby reducing the entropic penalty paid by the ligand in order to adopt the appropriate conformation to interact with Phe437.<sup>5m</sup>

While privileged analogues from the indazole class demonstrated promising in vitro profiles, suboptimal solubility and permeability precluded their use as in vivo tool compounds. Inhibitor 2, for example, had no measurable kinetic solubility in aqueous buffer (<1  $\mu$ M) and displayed poor permeability in MDCK cells ( $P_{app} = 0.1 \times 10^{-6}$  cm/s), which translated into unmeasurable bioavailability when dosed orally as a methocel suspension in rats, dogs, or mice, despite demonstrating IV clearance well below liver blood flow. Furthermore, inhibition of Aurora kinases proved problematic for this series (e.g., Aurora A  $K_i = 72$  nM for inhibitor 2), which we deemed a significant safety liability given the role for this family of kinases in mitotic regulation and broad cellular proliferation.<sup>14</sup>

We chose to address solubility concerns as our top priority and with an eye toward exploring structural changes that had the possibility of addressing selectivity improvements simultaneously. In a recent publication by scientists from GlaxoSmithKline, a simple metric termed “solubility forecast index” (SFI) was introduced to help predict solubility during the design phase and thus increase the probability that synthesized inhibitors demonstrate acceptable solubility characteristics.<sup>15</sup> We retrospectively applied this metric, calculated by the simple sum of aromatic ring count and the calculated log  $D$  at pH 7.4 ( $\text{clog}D_{7.4}$ ),<sup>16</sup> to analogues prepared in the indazole series (such as those exemplified in ref 5m) and found that solubility decreased with increasing SFI (Figure 3A). Although most analogues in this series had solubility forecast index greater than 6 and poor solubility, it was gratifying to observe that the vast majority of analogues with SFI less than 6 had acceptable solubility characteristics. Unfortunately, within the indazole structural class, the majority of analogues with SFI less than 6 showed poor ITK inhibition (Figure 3B). We were thus inspired to investigate scaffold modifications that would reduce the aromatic ring count, and thus the solubility forecast index, with an eye toward increasing the probability of improved solubility without sacrificing potency.

Examination of the indazole crystal structure (Figure 2) suggested that the indazole core would be the most promising candidate for saturation, as this ring makes no direct contact with the protein. While we were cognizant that this may disrupt the trajectory of the 6-pyrazole toward Phe435 and Lys391, we considered this an opportunity rather than a liability: we hoped that through this rescaffolding effort we would identify an alternative substituent to the pyrazole. While this substituent was clearly beneficial for ITK potency (cf. Figure 1), a

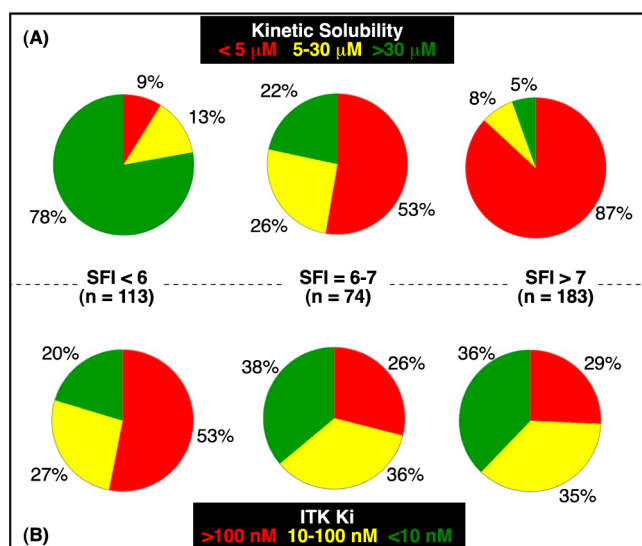
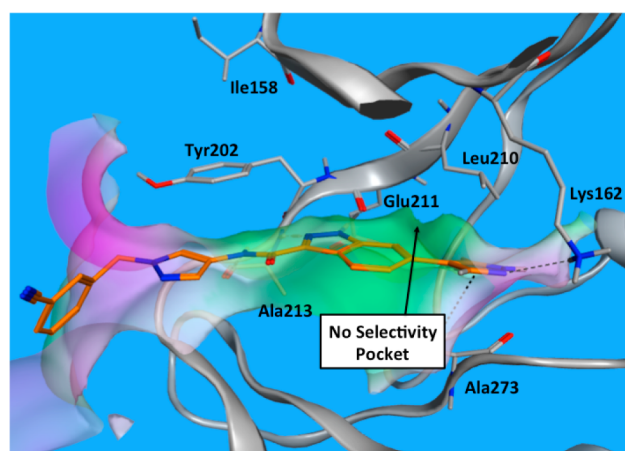


**Figure 3.** Relationship between solubility forecast index and kinetic solubility (A) and ITK potency (B) for the indazole class of ITK inhibitors.

significant portion of this potency was likely driven by the H-bond interaction with Lys391, the catalytic lysine that is highly conserved across the kinome, and thus is not likely optimal with respect to selectivity. Further, while the face-to-face  $\pi$ -stacking interaction with Phe435 might be considered beneficial for selectivity given the relative scarcity of phenylalanine gatekeeper residues, literature evidence suggests that pyrazole substitution in this region is beneficial for kinases with lipophilic nonaromatic gatekeeper residues, such as leucine present in the Aurora family.<sup>17</sup> Finally, the pyrazole moiety contributed negatively to the overall pharmaceutical property profile of our inhibitors, adding an aromatic ring, a hydrogen bond donor, and 29 Å<sup>2</sup> to the TPSA.

From a structural standpoint, we were most excited about the potential to occupy a lipophilic pocket adjacent to Phe435, evident in surface representations of all internal and published<sup>18</sup> ITK crystal structures. This pocket (Figure 2B), formed by the side chains of Phe435, Lys391, Val377, and Ala389, lies directly above the 6-position of the indazole core. The aromatic nature of the indazole provides no out-of-plane vector toward this pocket, but we envisioned that saturation of this region would introduce appropriate three-dimensionality to access this space. Furthermore, we obtained a crystal structure of inhibitor 2 bound to Aurora A, and no such pocket was evident, supporting the exploration of this region of space as a means to improve kinase selectivity (Figure 4).

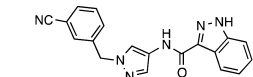
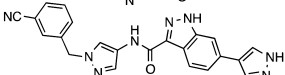
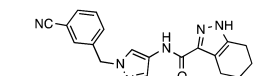
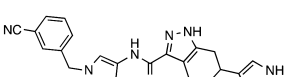
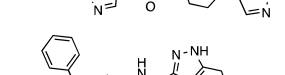
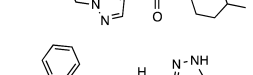
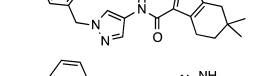
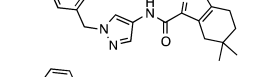
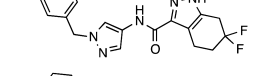
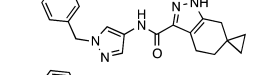
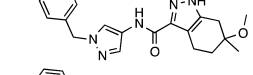
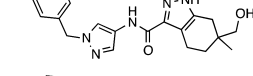
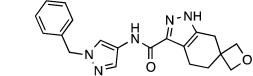
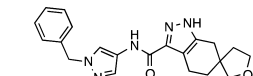
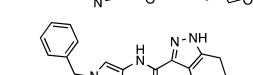
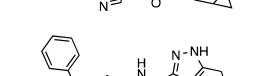
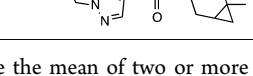
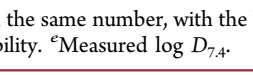
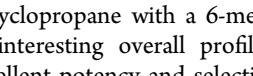
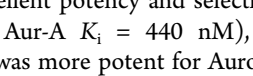
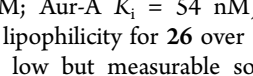
Table 1 summarizes the first round of optimization of the tetrahydroindazole series, which focused on the SAR around the THI core itself (eastern fragment). Inhibitor 14 (ITK  $K_i$  = 31 nM) served as an important proof-of-concept for this strategy, in that enzymatic potency was maintained via saturation of the six-membered ring of the indazole nucleus when compared to the progenitor indazole 1 (ITK  $K_i$  = 43 nM). Gratifyingly, kinetic solubility also trended in the right direction (14 vs 5.8  $\mu\text{M}$ ). As was the case for the indazole series, 3-pyrazolyl substitution at the 6-position did result in a potency increase (ITK  $K_i$  = 8.3 nM for enantiomer 15;  $K_i$  = 9.4 nM for enantiomer 15'), however, the increase was much less dramatic than that observed for the indazole series (1  $\rightarrow$  2). We postulate that this difference is due to the  $\text{sp}^3$  nature of the



**Figure 4.** Co-crystal structure of 2 with the kinase domain of Aurora A. Interactions and surface depiction are the same as for Figure 2

carbon at the 6-position of the THI core, which affects the ground-state torsion of the pyrazole ring relative to the core, orienting the heterocycle in a less-than-optimal configuration with respect to Phe435. We thus sought to explore nonaromatic lipophilic substitutions. We chose to carry out these investigations with simple benzyl substitution (instead of *m*-cyanobenzyl) of the western pyrazole since our previous SAR studies in the indazole series showed the cyano moiety offered little to no benefit.<sup>5m</sup> Monomethyl substitution was tolerated (inhibitors 16 and 16') but offered no significant benefit over the unsubstituted THI 14. Our first breakthrough occurred when *gem*-dimethyl substitution was added at the 6-position, yielding inhibitor 17 (ITK  $K_i$  = 5.3 nM) that was approximately 6-fold more potent than the unsubstituted analogue 14.<sup>19</sup> Gratifyingly, this ITK potency increase was not accompanied by significant increase in Aurora A inhibition. Verifying that this potency increase was not simply the result of nonspecific lipophilic interactions, *gem*-dimethyl substitution at the 5-position (18) offers no benefit relative to 14. *gem*-Difluoro substitution of the six-position was not well tolerated (19; ITK  $K_i$  = 180 nM), and *spiro*-cyclopropyl substitution results in poor Aurora A selectivity (20; Aur-A/ITK = 18). While the ITK potency increase observed for 17 was clearly promising, we were disheartened that solubility issues remained apparent, and we hypothesized that this was the source of the large enzyme-to-cell shift observed for this inhibitor, as measured by inhibition of the phosphorylation of PLC $\gamma$ , the direct substrate of ITK (IC<sub>50</sub> = 5200 nM). We believed, however, that this poor solubility was driven predominantly by the high lipophilicity of this inhibitor ( $\log D_{7.4}$  = 4.3), rather than the high aromatic ring count intrinsic to the indazole series. To address this concern, we explored introduction of oxygenation in the region of the *gem*-dimethyl group of 17. We speculated this strategy had the possibility to offer selectivity benefits as well because there was the potential of projecting a hydrogen bond donor or acceptor in the region of Ser499 (cf. Figure 2), a residue relatively unique to ITK. While oxygenation clearly reduced lipophilicity and increased solubility (inhibitors 21–24 all showed kinetic solubility >20  $\mu\text{M}$ ), only 6-methyl-6-hydroxymethyl substitution present in 22 was beneficial for ITK potency. Gratifyingly, although this inhibitor was slightly less potent than the *gem*-dimethyl inhibitor 17 (8.0 vs 5.3 nM), the cellular potency of 22 increased significantly (PLC $\gamma$  IC<sub>50</sub> = 530 nM), a presumed consequence of the improved solubility. Finally, combining a

Table 1. Structure–Activity Relationships for THI Eastern Fragment Optimization<sup>a</sup>

Inhibitor <sup>b</sup>	ITK K <sub>i</sub> (nM)	PLCγ IC <sub>50</sub> (nM)	Aur-A K <sub>i</sub> (nM) [fold over ITK]	SFI <sup>c</sup>	Solubility (μM) <sup>d</sup>	logD <sub>7.4</sub> <sup>e</sup>	
	<b>1</b>	43	---	870 [20X]	6.6	5.8	3.0
	<b>2</b>	1.1	210	72 [65X]	7.8	<1	3.4
	<b>14</b>	31	---	780 [26X]	5.4	14	2.6
	<b>15</b>	8.3	1700	210 [25X]	6.2	<1	2.5
	<b>15'</b>	9.4	2200	220 [23X]	6.2	<1	2.4
	<b>16</b>	22	930	1100 [50X]	6.0	<1	4.0
	<b>16'</b>	83	---	520 [6X]	6.0	<1	4.0
	<b>17</b>	5.3	5200	480 [90X]	6.3	<1	4.3
	<b>18</b>	69	---	1700 [24X]	6.3	<1	4.3
	<b>19</b>	180	---	950 [5X]	5.7	<1	3.8
	<b>20</b>	10	950	180 [18X]	5.8	<1	3.9
	<b>21</b>	180	---	---	5.6	77	2.2
	<b>21'</b>	280	---	---	5.6	29	2.2
	<b>22</b>	8.0	530	2300 [290X]	5.1	77	2.6
	<b>22'</b>	130	---	200 [1.5X]	5.1	83	2.7
	<b>23</b>	75	---	2900 [39X]	4.8	78	2.4
	<b>24</b>	42	---	>5700 [>100X]	5.2	20	2.2
	<b>24'</b>	55	---	---	5.2	60	2.2
	<b>25</b>	37	7100	2000 [54X]	5.4	13	2.5
	<b>25'</b>	190	---	870 [4.5X]	5.4	18	2.0
	<b>26</b>	3.0	410	440 [150X]	5.7	1.3	3.8
	<b>26'</b>	200	---	54 [0.3 X]	5.7	1.6	3.8

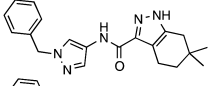
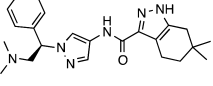
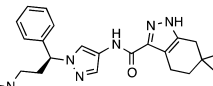
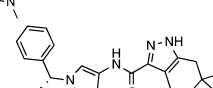
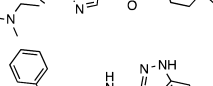
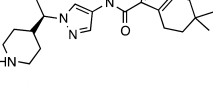
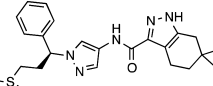
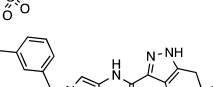
<sup>a</sup>All values are the mean of two or more independent assays (see Experimental Section for assay details). <sup>b</sup>For chiral inhibitors, the enantiomeric pairs are given the same number, with the less potent isomer given the “prime” distinction (e.g., **14** and **14'**). <sup>c</sup>SFI = clogD<sub>7.4</sub> + aromatic ring count.<sup>13</sup> <sup>d</sup>Kinetic solubility. <sup>e</sup>Measured log D<sub>7.4</sub>.

5–6 fused cyclopropane with a 6-methyl group (**26** and **26'**) yielded an interesting overall profile, with one enantiomer showing excellent potency and selectivity for ITK (**26**: ITK K<sub>i</sub> = 3.0 nM; Aur-A K<sub>i</sub> = 440 nM), whereas the alternative enantiomer was more potent for Aurora A than ITK (**26'**: ITK K<sub>i</sub> = 200 nM; Aur-A K<sub>i</sub> = 54 nM). Intriguingly, the small reduction in lipophilicity for **26** over **17** (log D<sub>7.4</sub> = 3.8 vs 4.3) translates to low but measurable solubility (1.3 μM) and a

concomitant increase in cellular potency (PLCγ IC<sub>50</sub> = 410 nM).

In a second phase of optimization, we explored benzylic and aromatic substitution of the western fragment (Table 2). To limit stereochemical complexity, we chose to explore this optimization using the 6-*gem*-dimethyl substitution in the eastern THI fragment. As was observed previously in the indazole series,<sup>5m</sup> introduction of a basic amine tail to the

Table 2. Optimization of the Western Fragment of the Tetrahydroindazole Series<sup>a</sup>

Inhibitor <sup>b</sup>	ITK $K_i$ (nM)	PLC $\gamma$ IC <sub>50</sub> (nM)	Aur-A $K_i$ (nM) [fold over ITK]	Solubility ( $\mu$ M) <sup>c</sup>	logD <sub>7.4</sub> <sup>d</sup>	MDCK Perm ( $P_{app}$ ; $10^{-6}$ cm/s)	
	17	5.3	5200	480 [90X]	<1	4.3	7.6
	27	0.8	38	210 [260X]	42	2.7	8.1
	28	0.7	55	460 [660X]	68	2.0	4.6
	28'	15	520	170 [11X]	49	2.0	---
	29	0.2	870	19 [95X]	102	1.3	0.1
	30	6.2	310	2100 [340X]	14	2.5	3.2
	31	0.7	47	500 [710X]	72	2.4	4.3
	32	1.2	113	290 [240X]	25	2.7	---

<sup>a</sup>All values are the mean of two or more independent assays (see Experimental Section for assay details). <sup>b</sup>Stereochemistry of **28** and **28'** assigned by X-ray structure of **28** (vide infra); all others assigned by analogy (only more potent enantiomer shown). <sup>c</sup>Kinetic solubility. <sup>d</sup>Measured log  $D_{7.4}$ .

benzylic substituent of the western fragment resulted in a significant increase in ITK potency and solubility. This was true for either a one-carbon (**27**; ITK  $K_i$  = 0.8 nM; solubility = 42  $\mu$ M) or two-carbon tail (**28**; 0.7 nM; solubility = 68  $\mu$ M). More importantly, this increase in ITK potency did not result in a significant increase in potency for Aurora A. Furthermore, cellular potency is increased by an even larger margin (PLC $\gamma$  IC<sub>50</sub> = 38 and 55 nM, respectively) relative to the unsubstituted comparator **17**, which we postulate is driven by solubility because permeability is relatively unchanged.<sup>20</sup> It is interesting to note that the enantiomer of **28** (**28'**; ITK  $K_i$  = 15 nM) loses potency for ITK and gains potency for Aurora A ( $K_i$  = 170 nM) relative to **17**. Taken together, these data reinforce the hypothesis that the potency increase is driven by reinforcement of the binding conformation for the more potent enantiomer, positioning the phenyl group appropriately to interact with Phe437. Increasing the size of the benzylic substituent, such as the piperidyl analogue **29**, results in a further boost in ITK potency (ITK  $K_i$  = 0.2 nM), but this is not captured in increased cellular potency (PLC $\gamma$  IC<sub>50</sub> = 870 nM), presumably due to the poor permeability of this analogue ( $0.1 \times 10^{-6}$  cm/s). Nonbasic solubilizing groups such as sulfone **30** were also tolerated, and while no ITK potency increase is evident enzymatically (ITK  $K_i$  = 6.2 nM), cellular potency was increased relative to **17** (PLC $\gamma$  IC<sub>50</sub> = 310 nM), driven by

the increase in solubility (14  $\mu$ M). Small lipophilic substituents were tolerated on the phenyl ring (e.g., **31** and **32**) but offered no significant benefit over the unsubstituted phenyl ring.

An X-ray crystal structure of inhibitor **28** bound to the active site of ITK was obtained (Figure 5) and revealed that the inhibitor binds to the enzyme as designed. The axial methyl

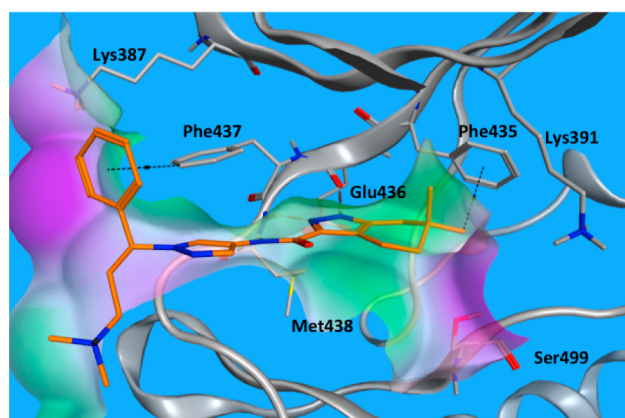


Figure 5. Co-crystal structure of **28** with the kinase domain of ITK. Interactions and surface depictions are the same as for Figure 2

Table 3. In Vivo Pharmacokinetic Parameters for Inhibitor 28 (GNE-9822)<sup>a</sup>

species	route	vehicle	dose volume (mL/kg)	dose (mg/kg)	C <sub>max</sub> (μM)	AUC (μM·h)	Cl (mL/min/kg)	T <sub>1/2</sub> (h)	V <sub>ss</sub> (L/kg)	%F
mouse (BALB/c)	IV	SEDDS <sup>b</sup>	1.0	1.0		1.5	40	2.9	10	
	PO	Crem/Cit <sup>c</sup>	5.0	50	3.8	27				36
rat (Sprague–Dawley)	IV	SEDDS	1.0	1.0		0.6	70	3.0	14	
	PO	SEDDS	2.0	5.0	0.2	1.1				40
dog (beagle)	IV	SEDDS	1.0	1.0		1.9	21	5.4	6.7	
	PO	SEDDS	0.5	5.0	0.9	10				100

<sup>a</sup>All values are the mean from at least two animals. <sup>b</sup>SEDDS = self-emulsifying drug delivery system (1 part [50% cremophor, 35% NMP, 15% Miglyol], 3 parts water). <sup>c</sup>Crem/Cit = 5% cremophor in 50% citric acid.

group of the THI core projects into the lipophilic pocket adjacent to Phe435, and the equatorial methyl group also makes lipophilic contact with the phenyl group of this residue. As with the indazole series, the inhibitor maintains three hydrogen bonds with the hinge region, and the benzylic stereocenter orients the western phenyl group for an appropriate edge-to-face  $\pi$ -stack with Phe437.

Given its promising preliminary profile, inhibitor 28 (also known as GNE-9822) was subjected to additional in vitro and in vivo characterization. Broad kinase selectivity of this molecule was observed: only six of 286 off-target kinases<sup>21</sup> were inhibited >70% when tested at 0.1 μM (>100X ITK K<sub>i</sub>). In addition to the good solubility and moderate permeability disclosed above, other in vitro ADME properties were promising, with 28 demonstrating low clearance in human hepatocytes (Cl<sub>Hep</sub> = 5.0 mL/min/kg) and moderate plasma protein binding (hPPB = 93%). In vivo ADME properties (Table 3) were acceptable, with good bioavailability and half-lives observed in all preclinical species, albeit with moderate (mouse, dog) to high (rat) clearance.

To demonstrate the advantages afforded by saturation of the indazole nucleus, a collection of potency, selectivity, and calculated and measured pharmaceutical properties and ADME data are summarized in Table 4 for the top indazole 3 and tetrahydroindazole 28. Although enzymatic and cellular potency of 3 is marginally superior, the lower molecular weight of 28 results in the two inhibitors showing equivalent ligand efficiency.<sup>23</sup> Kinase selectivity clearly favors 28, whether measured as inhibition of our sentinel off-target Aurora A or in terms of a broader kinase panel. Although both molecules show acceptable kinetic solubility, permeability of 28 is greatly improved, resulting in a dramatic improvement in bioavailability.

In conclusion, we have evolved a previously disclosed indazole series of inhibitors through saturation of a core aromatic ring to yield a related but distinct tetrahydroindazole inhibitor class. This new chemical matter demonstrates improved selectivity and pharmaceutical properties, specifically solubility and permeability, when compared to their progenitors. Future publications will disclose further improvements on this chemical matter in the areas of potency, selectivity, and ADME properties.

## EXPERIMENTAL SECTION

**Chemistry.** *General.* All commercially available reagents and solvents were used as received. Reactions using air- or moisture-sensitive reagents were performed under an atmosphere of N<sub>2</sub> using freshly opened EMD DriSolv solvents. Reaction progress was monitored by TLC and/or HPLC. Flash chromatography was

Table 4. Comparison of Overall Profiles of Indazole 3 and THI 28

	Indazole 3	THI 28 GNE-9822
MW	455 g/mol	421 g/mol
ITK K <sub>i</sub>	0.1 nM	0.7 nM
LE <sub>ITK K<sub>i</sub></sub> <sup>a</sup>	0.40	0.40
PLCγ IC <sub>50</sub>	25 nM	55 nM
Aur-A K <sub>i</sub> [fold]	15 nM [150]	460 nM [660]
Kinase Sel. <sup>b</sup>	58/218	6/286
Solubility	94 μM	68 μM
SI	6.8	5.0
logD <sub>7.4</sub>	1.9	2.8
MDCK Perm.	0.3 × 10 <sup>-6</sup> cm/s	4.6 × 10 <sup>-6</sup> cm/s
TPSA	107	78
hPPB	97	93
HHep Cl <sup>c</sup>	5.1 mL/min/kg	5.0 mL/min/kg
Rat %F <sup>d</sup>	0	40

<sup>a</sup>Ligand efficiency = 1.4 × (-log<sub>10</sub>(ITK K<sub>i</sub>))/(no. of heavy atoms).<sup>20</sup>

<sup>b</sup>Number of kinases inhibited >70% at 0.1 μM in an Invitrogen panel.

<sup>c</sup>Clearance in human hepatocytes. <sup>d</sup>Dosed PO at 5 mg/kg as a solution.

performed with Isco CombiFlash Companion systems using prepacked silica gel columns (40–60 μm particle size RediSep or 20–40 μm spherical silica gel RediSep Gold columns, or similar columns from other vendors). Preparative HPLC purifications were performed on a Varian Prostar instrument, using a Phenomenex Gemini-NX C-18 (0.3 cm × 5 cm; 5 μM) stationary phase, with 0.1% aqueous formic acid/ acetonitrile or 0.1% aqueous ammonium hydroxide/acetonitrile gradients as the mobile phase (typically 5–85% acetonitrile over 10 min) with a flow rate of 60 mL/min. Preparative SFC separations were performed on a PIC Solutions instrument, with conditions indicated in the Experimental Section. NMR spectra were measured on Bruker 300 or 400 MHz spectrometers, and chemical shifts are reported in ppm downfield from TMS using residual nondeuterated solvent as internal standards (CHCl<sub>3</sub>, 7.26 ppm; DMSO, 2.50 ppm; MeOH, 3.31 ppm). High-resolution mass spectrometry of final compounds were performed on a Thermo UHPLC/QE with a Thermo-Q Exactive mass spectrometry detector using ESI ionization, after elution on a Acquity BEH C18 (2.1 mm × 50 mm; 1.7 μm particle size) stationary phase using a gradient of water/acetonitrile (3–97% over 7 min; 0.1% formic acid in both phases). The purity of final compounds 14–32 was verified by HPLC on an Agilent 1200 instrument with an Agilent SB

C-18 (2.1 mm × 30 mm; 1.8 μm particle size) stationary phase, and a gradient of water/acetonitrile (5–95% over 6 min; 0.05% TFA in both phases) at a flow rate of 0.4 mL/min. Quantification of target and impurities was done by UV detection at 254 nm, and is >95% in all cases.

**General Procedure A: Formation of Pyrazole Carboxylic Acids 8 or 10 via Claisen Condensation. Step 1.** To a solution of ketone 4 or 9 (1.0 equiv) in EtOH (0.5 mL/mmol) was added NaOEt (21 wt % solution in EtOH; 1.1 equiv) and diethyl oxalate (1.0 equiv) at room temperature. After stirring overnight, the mixture was concentrated in vacuo and used directly without purification.

**Step 2.** The residue from step 1 was diluted with acetic acid (0.5 mL/mmol), cooled to 0 °C, and hydrazine hydrate (1.1 equiv) was added. The mixture was warmed to room temperature, stirred for 1 h, and then was diluted with satd NaHCO<sub>3</sub>(aq) and extracted with 10% MeOH/CH<sub>2</sub>Cl<sub>2</sub>. The organic extracts were dried (MgSO<sub>4</sub>) and concentrated in vacuo. Purification by CombiFlash using a mixture of heptane and EtOAc provided the intermediate ethyl pyrazole carboxylates.

**Step 3.** The ethyl pyrazole carboxylate obtained in step 2 was diluted with THF (20 mL/mmol) and cooled to 0 °C and sodium hydride (60 wt %; 3.0 equiv) was added. After stirring for 1 h at 0 °C, SEM-Cl (1.2 equiv) was added and the mixture was allowed to warm to room temperature overnight. Excess hydride was quenched by the careful addition of water, and then the mixture was diluted with additional water and extracted three times with EtOAc. The combined organic extracts were dried (MgSO<sub>4</sub>) and concentrated in vacuo. Intermediate SEM protected ethyl pyrazole carboxylates were then obtained by purification by CombiFlash using a mixture of EtOAc and heptane. These esters were diluted with THF (6 mL/mmol), acetonitrile (6 mL/mmol), and water (6 mL/mmol). Lithium hydroxide monohydrate (7 equiv) was then added, and the mixture stirred overnight at rt. After dilution with additional water, the mixture was acidified to pH 3 with 1 N HCl(aq), and then extracted three times with 10% MeOH/CH<sub>2</sub>Cl<sub>2</sub>. The combined organic extracts were dried (MgSO<sub>4</sub>) and concentrated in vacuo to provide the title compounds of sufficient purity to be used directly.

**General Procedure B: Formation of Pyrazole Carboxylic Acids 6 via Diazoacetate Addition/Rearrangement. Step 1.** A solution of diisopropylamine (1.7 equiv) in THF (5 mL/mmol) was cooled to –78 °C, and a solution of *n*-butyl lithium in hexanes (1.6 M; 1.5 equiv) was added. After stirring for 5 min, this mixture was added via cannula to a –78 °C solution of ethyl diazoacetate (1.6 equiv) and ketone 4 in THF (5.0 mL/mmol). After stirring for 1 h at –78 °C, the reaction was quenched by the addition of satd NH<sub>4</sub>Cl(aq). The mixture was warmed to room temperature, diluted with water, and extracted twice with EtOAc. The combined organic extracts were dried (MgSO<sub>4</sub>) and concentrated in vacuo. Purification by CombiFlash with a mixture of heptane and EtOAc as the eluent provided the intermediate ethyl 2-diazo-2-hydroxycyclohexanyl-acetates.

**Step 2.** The ethyl 2-diazo-2-hydroxycyclohexanyl-acetate from step 1 was diluted with pyridine (4 mL/mmol), and then POCl<sub>3</sub> (4.0 equiv), and the mixture was stirred overnight at room temperature. After in vacuo concentration, the mixture was poured onto ice and extracted three times with EtOAc. The combined organic extracts were dried (MgSO<sub>4</sub>) and concentrated in vacuo. This residue was diluted with *n*-octane (2 mL/mmol) and heated to 110 °C overnight. After in vacuo concentration, purification by CombiFlash with a mixture of heptane and EtOAc provided the intermediate ethyl pyrazole carboxylate.

**Step 3.** The ethyl pyrazole carboxylate obtained in step 2 was reacted in a manner identical to step 3 of general procedure A above, to provide the title compounds.

**General Procedure C: Formation of Nitropyrazoles 12 via Benzyl Bromide Alkylation.** To a solution of 4-nitro-1H-pyrazole (1.0 equiv) in DMF (6 mL/mmol) was added K<sub>2</sub>CO<sub>3</sub> (1.2 equiv) and benzyl bromide 11i or 11ii (1.0 equiv). After stirring overnight at room temperature, the mixture was diluted with EtOAc and washed twice with 1:1 H<sub>2</sub>O:brine. The organic extracts were dried (Na<sub>2</sub>SO<sub>4</sub>) and

concentrated in vacuo. Purification by CombiFlash with a mixture of EtOAc and heptane provided the title compounds.

**General Procedure D: Formation of Nitropyrazoles 12 via Mitsunobu Reaction.** A solution of benzylic alcohols 11iii–viii (1.0 equiv) in THF (2 mL/mmol) was cooled to 0 °C, and then 4-nitro-1H-pyrazole (1.0 equiv), PPh<sub>3</sub> (2.0 equiv), and diethyl azodicarboxylate (2.0 equiv) were added sequentially. The mixture was allowed to warm to room temperature overnight, and then the mixture was concentrated in vacuo. The residue was purified by CombiFlash with a mixture of heptane and EtOAc to provide the title compounds, occasionally contaminated with triphenylphosphine oxide of varying quantities. Yields are assumed to be quantitative for purpose of downstream chemistry quantities, and this reagent is used in excess.

**General Procedure E: Formation of Target Compounds 14 and 15. Step 1.** To a solution of 3-((4-nitro-1H-pyrazol-1-yl)methyl)benzonitrile (12i) (1.0 equiv) in ethanol (7 mL/mmol) was added NH<sub>4</sub>Cl (5.0 equiv) as a saturated solution in water then iron (5.0 equiv). The mixture was heated to 80 °C for 60 min and then cooled to room temperature. The mixture was diluted with EtOAc and washed with satd NaHCO<sub>3</sub>(aq) and brine. The organic extracts were dried (Na<sub>2</sub>SO<sub>4</sub>) and concentrated in vacuo to provide 3-((4-amino-1H-pyrazol-1-yl)methyl)benzonitrile (13i), which was used without purification.

**Step 2.** To a solution of pyrazole carboxylic acid 6i or 6ii (1.0 equiv) and aminopyrazole 13i (1.5 equiv) in DMF (3 mL/mmol) was added TBTU (1.4 equiv) and iPr<sub>2</sub>NEt (3.0 equiv), and the mixture was stirred overnight at rt. After dilution with water, the mixture was extracted three times with EtOAc, and then the combined organic extracts were dried (MgSO<sub>4</sub>) and concentrated in vacuo. Purification by CombiFlash with an EtOAc and heptane mixture provided the SEM protected title compounds.

**Step 3.** The product of step 2 was diluted with 4 N HCl in dioxane (15 mL/mmol) and heated to 60 °C for 1 h. After cooling to room temperature and in vacuo concentration, the residue was diluted with EtOH (30 mL/mmol) and 5 M NaOH(aq) (12 mL/mmol) and stirred for an additional hour to remove a residual *N*-hydroxymethylation of the pyrazole. The mixture was diluted with water, extracted three times with 10% MeOH/CH<sub>2</sub>Cl<sub>2</sub>, dried (MgSO<sub>4</sub>), and concentrated in vacuo. Mass directed reverse-phase HPLC purification, followed by lyophilization, provided the title compounds. For samples possessing stereogenicity, racemic mixtures were resolved into single enantiomers using SFC purification (or preparative HPLC) on chiral stationary phases as indicated.

**General Procedure F: Formation of Target Compounds 16–32. Step 1.** To a solution of benzylated nitro pyrazoles 12 (1.0 equiv; may contain O=PPh<sub>3</sub>) in ethanol (3 mL/mmol) was added palladium on carbon (10 wt %; 50 mg/mmol), and the mixture was stirred under an atmosphere of hydrogen overnight. The sample was then purged with nitrogen, the catalyst was deactivated by the addition of CH<sub>2</sub>Cl<sub>2</sub>, and the mixture was filtered through Celite. Concentration in vacuo provided the intermediate aminopyrazoles 13, which were used without purification.

**Steps 2 and 3.** To a solution of pyrazole carboxylic acid 6, 8, or 10 (1.0 equiv) and aminopyrazole 13 (1.5 equiv; may contain O=PPh<sub>3</sub>) were reacted according to steps 2 and 3 of general procedure E to provide the title compounds.

1-((2-(Trimethylsilyl)ethoxy)methyl)-4,5,6,7-tetrahydro-1H-indazole-3-carboxylic Acid (6i). Cyclohexanone (4i; commercial) was reacted according to general procedure B to provide 6i in 10% yield over the three steps. <sup>1</sup>H NMR (400 MHz, DMSO) δ 12.45 (s, 1H), 5.36 (s, 2H), 3.51 (t, J = 7.9, 2H), 2.66–2.58 (m, 4H), 1.78–1.61 (m, 4H), 0.82 (t, J = 7.9, 2H), –0.05 (s, 9H).

1-((2-(Trimethylsilyl)ethoxy)methyl)-6-((2-(trimethylsilyl)ethoxy)methyl)-1H-pyrazol-4-yl)-4,5,6,7-tetrahydro-1H-indazole-3-carboxylic Acid (6ii). 4-(1-((2-(Trimethylsilyl)ethoxy)methyl)-1H-pyrazol-4-yl)cyclohexanone (4ii)<sup>7</sup> was reacted according to general procedure B, to provide 6ii in 43% yield over the three steps. <sup>1</sup>H NMR (400 MHz, CDCl<sub>3</sub>) δ 7.47–7.33 (m, 2H), 5.40–5.34 (m, 2H), 3.78–3.51 (m, 4H), 3.18–1.49 (m, 9H), 0.96–0.65 (m, 4H), 0.02 – –0.14 (m, 18H).

**6-Methyl-1-((2-(trimethylsilyl)ethoxy)methyl)-4,5,6,7-tetrahydro-1H-indazole-3-carboxylic Acid (6iii).** 4-Methylcyclohexanone (**4iiv**; commercial) was reacted according to general procedure B, to provide **6iii** in 32% yield over the three steps.  $^1\text{H NMR}$  (400 MHz,  $\text{CDCl}_3$ )  $\delta$  5.39 (s, 2H), 3.59–3.52 (m, 2H), 2.98–2.88 (m, 1H), 2.81 (dd,  $J = 16.2, 5.3$ , 1H), 2.70–2.59 (m, 1H), 2.23 (dd,  $J = 16.2, 9.6$ , 1H), 2.02 (s, 1H), 1.99–1.84 (m, 2H), 1.44–1.32 (m, 1H), 1.11 (d,  $J = 6.6$ , 3H), 0.93–0.85 (m, 2H), –0.02 (s, 9H).

**6,6-Dimethyl-1-((2-(trimethylsilyl)ethoxy)methyl)-4,5,6,7-tetrahydro-1H-indazole-3-carboxylic Acid (6iv).** 4,4-Dimethylcyclohexanone (**4iv**; commercial) was reacted according to general procedure B, to provide **6iv** in 50% yield over the three steps.  $^1\text{H NMR}$  (400 MHz,  $\text{CDCl}_3$ )  $\delta$  5.39 (s, 2H), 3.58–3.50 (m, 2H), 2.77 (t,  $J = 6.4$ , 2H), 2.45 (s, 2H), 2.03 (s, 1H), 1.54 (t,  $J = 6.4$ , 2H), 1.02 (s, 6H), 0.91–0.83 (m, 2H), –0.03 (s, 9H).

**6,6-Difluoro-1-((2-(trimethylsilyl)ethoxy)methyl)-4,5,6,7-tetrahydro-1H-indazole-3-carboxylic Acid (6v).** 4,4-Difluorocyclohexanone (**4v**; commercial) was reacted according to general procedure B, to provide **6v** in 41% yield over the three steps.  $^1\text{H NMR}$  (400 MHz,  $\text{CDCl}_3$ )  $\delta$  5.43 (s, 2H), 3.59–3.52 (m, 2H), 3.24 (t,  $J = 13.2$ , 2H), 3.00 (t,  $J = 6.6$ , 2H), 2.29–2.16 (m, 2H), 2.03 (s, 1H), 0.92–0.86 (m, 2H), –0.02 (s, 9H).

**1'-((2-(Trimethylsilyl)ethoxy)methyl)-1',4',5',7'-tetrahydrospiro[cyclopropane-1,6'-indazole]-3'-carboxylic Acid (6vi).** Spiro[2.5]-octan-6-one (**4vi**; commercial) was reacted according to general procedure B to provide **6vi** in 31% yield over the three steps.  $^1\text{H NMR}$  (400 MHz,  $\text{CDCl}_3$ )  $\delta$  5.37 (s, 2H), 3.60–3.51 (m, 2H), 2.83 (t,  $J = 6.2$ , 2H), 2.55 (s, 2H), 2.11 (s, 1H), 1.55 (t,  $J = 6.2$ , 2H), 0.91–0.84 (m, 2H), 0.51–0.46 (m, 2H), 0.45–0.40 (m, 2H), –0.03 (s, 9H).

**6-Methoxy-6-methyl-1-((2-(trimethylsilyl)ethoxy)methyl)-4,5,6,7-tetrahydro-1H-indazole-3-carboxylic Acid (6vii).** 4-Methoxy-4-methylcyclohexanone (**4vii**)<sup>24</sup> was reacted according to general procedure B to provide **6vii** in 43% yield over the three steps.  $^1\text{H NMR}$  (400 MHz,  $\text{CDCl}_3$ )  $\delta$  3.58–3.51 (m, 2H), 3.25 (s, 3H), 2.88 (d,  $J = 16.4$  Hz, 1H), 2.80 (t,  $J = 6.3$  Hz, 2H), 2.63 (d,  $J = 16.4$  Hz, 1H), 2.12–1.98 (m, 4H), 1.73–1.63 (m, 1H), 1.32 (s, 3H), 0.92–0.84 (m, 2H), –0.01 – –0.04 (m, 9H).

**6-((tert-Butyldimethylsilyloxy)methyl)-6-methyl-1-((2-(trimethylsilyl)ethoxy)methyl)-4,5,6,7-tetrahydro-1H-indazole-3-carboxylic Acid (6viii).** 4-((tert-Butyldimethylsilyloxy)methyl)-4-methylcyclohexanone (**4viii**)<sup>7</sup> was reacted according to general procedure B to provide **6viii** in 76% yield over the three steps.  $^1\text{H NMR}$  (400 MHz,  $\text{CDCl}_3$ )  $\delta$  5.39 (s, 2H), 3.57–3.51 (m, 2H), 3.42–3.35 (m, 2H), 2.83 (dt,  $J = 17.2, 5.5$ , 1H), 2.77–2.68 (m, 1H), 2.64 (d,  $J = 16.6$ , 1H), 2.35 (d,  $J = 16.4$ , 1H), 2.03 (s, 1H), 1.73–1.64 (m, 1H), 1.54–1.44 (m, 1H), 0.94 (s, 3H), 0.91–0.85 (m, 11H), 0.04 (s, 3H), 0.03 (s, 3H), –0.03 (s, 9H).

**1-((2-(Trimethylsilyl)ethoxy)methyl)-1,4,5,7-tetrahydrospiro[indazole-6,3'-oxetane]-3-carboxylic Acid (6ix).** 2-Oxaspiro[3.5]-nonan-7-one (**4ix**; commercial) was reacted according to general procedure B to provide **6ix** in 31% yield over the three steps. The dehydration step (step 2) was performed using modified conditions as follows: To a solution of ethyl 2-diazo-2-(7-hydroxy-2-oxaspiro[3.5]-nonan-7-yl)acetate (100 mg, 0.393 mmol) in  $\text{CH}_2\text{Cl}_2$  (2.5 mL) was added triethylamine (0.138 mL, 0.983 mmol) and trifluoroacetic anhydride (0.111 mL, 0.787 mmol). The mixture was stirred for 15 min and then diluted with  $\text{H}_2\text{O}$  and extracted with  $\text{CH}_2\text{Cl}_2$ . The combined organic extracts were dried ( $\text{MgSO}_4$ ) and concentrated in vacuo. The residue was used directly in step 3 without purification.  $^1\text{H NMR}$  (400 MHz,  $\text{CDCl}_3$ )  $\delta$  5.50 (s, 2H), 4.60 (d,  $J = 6.0$ , 2H), 4.48 (d,  $J = 6.0$ , 2H), 3.62–3.56 (m, 2H), 3.07 (s, 2H), 2.87 (t,  $J = 6.2$ , 2H), 2.15–2.06 (m, 3H), 0.92 (t,  $J = 8.2$ , 2H), –0.00 (s, 9H).

**1'-((2-(Trimethylsilyl)ethoxy)methyl)-1',4',5',7'-hexahydro-2H-spiro[furan-3,6'-indazole]-3'-carboxylic Acid (6x).** 2-Oxaspiro[4.5]decan-8-one (**4x**)<sup>7</sup> was reacted according to general procedure B to provide **6x** in 38% yield over the three steps.  $^1\text{H NMR}$  (400 MHz,  $\text{CDCl}_3$ )  $\delta$  5.45–5.37 (m, 2H), 3.98–3.91 (m, 2H), 3.63–3.51 (m, 4H), 2.89–2.77 (m, 2H), 2.76–2.63 (m, 2H), 2.03 (s, 1H), 1.93–1.69 (m, 4H), 0.91–0.85 (m, 2H), –0.03 (s, 9H).

**5,5-Dimethyl-1-((2-(trimethylsilyl)ethoxy)methyl)-4,5,6,7-tetrahydro-1H-indazole-3-carboxylic Acid (8iv).** 4,4-Dimethylcyclohexanone

(**4iv**; commercial) was reacted according to general procedure A to provide **8iv** in 46% yield over the three steps.  $^1\text{H NMR}$  (500 MHz,  $\text{CDCl}_3$ )  $\delta$  5.41 (s, 2H), 3.58–3.53 (m, 2H), 2.68 (t,  $J = 6.5$ , 2H), 2.57 (s, 2H), 1.60 (t,  $J = 6.5$ , 2H), 1.00 (s, 6H), 0.91–0.85 (m, 2H), –0.03 (s, 9H).

**1,4,4a,5,5a,6-Hexahydrocyclopropa[f]indazole-3-carboxylic Acid (10xi).** Bicyclo[4.1.0]heptan-3-one (**9xi**)<sup>25</sup> was reacted according to general procedure A, omitting the SEM protection step, to provide **10xi** in 11% yield over the three steps. Isomeric 3,4,5,6,6a-hexahydrocyclopropa[e]indazole-1-carboxylic acid was also obtained through this sequence and was separated from **10xi** by preparative HPLC. MS:  $m/z = 179$  [ $\text{M} + \text{H}$ ]<sup>+</sup>.

**5a-Methyl-1,4,4a,5,5a,6-hexahydrocyclopropa[f]indazole-3-carboxylic Acid (10xii).** 1-Methylbicyclo[4.1.0]heptan-3-one (**9xii**)<sup>27</sup> was reacted according to general procedure A, omitting the SEM protection step, to provide **10xii** in 33% yield over the three steps.  $^1\text{H NMR}$  (300 MHz, DMSO)  $\delta$  12.86 (br, 2H), 3.15–3.09 (d,  $J = 17.1$  Hz, 1H), 2.96–2.79 (m, 2H), 2.66–2.61 (d,  $J = 15.9$  Hz, 1H), 1.20 (s, 3H), 1.08–1.00 (m, 1H), 0.32–0.28 (m, 1H), 0.07–0.05 (m, 1H).

**3-((4-Nitro-1H-pyrazol-1-yl)methyl)benzonitrile (12i).** *m*-Cyanobenzyl bromide (**11i**; commercial) was reacted according to general procedure C to provide **12i** in 95% yield.  $^1\text{H NMR}$  (400 MHz,  $\text{CDCl}_3$ )  $\delta$  8.15 (s, 1H), 8.12 (s, 1H), 7.72–7.64 (m, 1H), 7.61–7.48 (m, 3H), 5.35 (s, 2H).

**1-Benzyl-4-nitro-1H-pyrazole (12ii).** Benzyl bromide (**11ii**; commercial) was reacted according to general procedure C to provide **12ii** in 97% yield.  $^1\text{H NMR}$  (400 MHz,  $\text{CDCl}_3$ )  $\delta$  8.10 (s, 1H), 8.04 (s, 1H), 7.45–7.36 (m, 3H), 7.33–7.27 (m, 2H), 5.31 (s, 2H).

***N,N*-Dimethyl-2-(4-nitro-1H-pyrazol-1-yl)-2-phenylethanamine (12iii).** 2-(Dimethylamino)-1-phenylethanol (**11iii**)<sup>26</sup> was reacted according to general procedure D to provide **12iii** contaminated with  $\text{O}=\text{PPh}_3$  (yield assumed to be 100% for downstream chemistry).  $^1\text{H NMR}$  (400 MHz, Chloroform-*d*)  $\delta$  8.29 (s, 1H), 8.11 (s, 1H), 7.42–7.24 (m, 5H), 5.44 (dd,  $J = 10.2, 4.7$  Hz, 1H), 3.40 (dd,  $J = 13.5, 10.2$  Hz, 1H), 2.80 (dd,  $J = 13.5, 4.7$  Hz, 1H), 2.30 (s, 6H).

***N,N*-Dimethyl-3-(4-nitro-1H-pyrazol-1-yl)-3-phenylpropan-1-amine (12iv).** 3-(Dimethylamino)-1-phenylpropan-1-ol (**11iv**)<sup>27</sup> was reacted according to general procedure D to provide **12iv** in 80% yield.  $^1\text{H NMR}$  (400 MHz,  $\text{CDCl}_3$ )  $\delta$  8.15 (s, 1H), 8.09 (s, 1H), 7.41–7.32 (m, 5H), 5.49 (dd,  $J = 8.5, 6.5$ , 1H), 2.65–2.54 (m, 1H), 2.34–2.24 (m, 1H), 2.20 (s, 6H), 2.19–2.14 (m, 2H).

***tert*-Butyl 4-((4-Nitro-1H-pyrazol-1-yl)(phenyl)methyl)piperidine-1-carboxylate (12v).** *tert*-Butyl 4-(hydroxy(phenyl)methyl)piperidine-1-carboxylate (**11v**)<sup>28</sup> was reacted according to general procedure D to provide **12v** in 51% yield.  $^1\text{H NMR}$  (400 MHz,  $\text{CDCl}_3$ )  $\delta$  8.17 (s, 1H), 8.10 (s, 1H), 7.47–7.32 (m, 5H), 4.76 (d,  $J = 10.7$  Hz, 1H), 4.23–3.98 (m, 2H), 2.75–2.57 (m, 3H), 1.44 (s, 9H), 1.40–1.03 (m, 4H).

**1-(3-(Methylsulfonyl)-1-phenylpropyl)-4-nitro-1H-pyrazole (12vi).** 1-(3-(Methylthio)-1-phenylpropyl)-4-nitro-1H-pyrazole was formed by subsection of 3-(methylthio)-1-phenylpropan-1-ol (**11vi**) to general procedure D, followed by the following sulfone oxidation step: *m*CPBA (5.0 g, 29 mmol, 2.5 equiv) was added in several portions to a stirred solution of 1-[3-(methylsulfonyl)-1-phenylpropyl]-4-nitro-1H-pyrazole (3.0 g, 10.8 mmol, 1.0 equiv) in dichloromethane (100 mL) at room temperature. The solids from the reaction were filtered out, and the filtrate was diluted with 300 mL of dichloromethane. The resulting mixture was washed with  $2 \times 150$  mL of saturated sodium carbonate, dried over anhydrous sodium sulfate, and concentrated under vacuum to provide the title compound in 79% yield from **11vi** that was used without further purification. MS:  $m/z = 310$  [ $\text{M} + \text{H}$ ]<sup>+</sup>.

***N,N*-Dimethyl-3-(4-nitro-1H-pyrazol-1-yl)-3-(*m*-tolyl)propan-1-amine (12vii).** 3-(Dimethylamino)-1-(*m*-tolyl)propan-1-ol (**11vii**)<sup>29</sup> was reacted according to general procedure D to provide **12vii** in 52% yield. MS:  $m/z = 289$  [ $\text{M} + \text{H}$ ]<sup>+</sup>.

**3-(3-Chlorophenyl)-*N,N*-dimethyl-3-(4-nitro-1H-pyrazol-1-yl)-propan-1-amine (12viii).** 1-(3-Chlorophenyl)-3-(dimethylamino)propan-1-ol (**11viii**)<sup>30</sup> was reacted according to general procedure D to provide **12viii** in 40% yield. MS:  $m/z = 309$  [ $\text{M} + \text{H}$ ]<sup>+</sup>.

*N*-(1-(3-Cyanobenzyl)-1*H*-pyrazol-4-yl)-4,5,6,7-tetrahydro-1*H*-indazole-3-carboxamide (**14**). **6i** and **12i** were reacted according to general procedure E to provide **14** in 49% yield. <sup>1</sup>H NMR (400 MHz, DMSO) δ 12.82 (s, 1H), 10.08 (d, *J* = 12.0, 1H), 8.16 (s, 1H), 7.77 (d, *J* = 6.8, 1H), 7.67 (s, 2H), 7.60–7.52 (m, 2H), 5.35 (s, 2H), 2.67 (t, *J* = 5.5, 2H), 2.61 (t, *J* = 5.8, 2H), 1.77–1.62 (m, 4H). HRMS *m/z* calcd for C<sub>19</sub>H<sub>19</sub>ON<sub>6</sub> [M + H]<sup>+</sup> 347.1615; found 347.1628.

*N*-(1-(3-Cyanobenzyl)-1*H*-pyrazol-4-yl)-5-(1*H*-pyrazol-4-yl)-4,5,6,7-tetrahydro-1*H*-indazole-3-carboxamide (**15** and **15'**). **6ii** and **12i** were reacted according to general procedure E to provide racemic **15**. SFC purification (Chiralpak OJ (21.2 mm × 250 mm, 5 μm particle size) at 35% MeOH w/0.1%NH<sub>4</sub>OH; 70 mL/min, 100 bar, 40 °C) provided **15** (6% yield) and **15'** (9% yield). **15**: <sup>1</sup>H NMR (400 MHz, DMSO) δ 12.88 (s, 1H), 12.58 (s, 1H), 10.14 (s, 1H), 8.17 (s, 1H), 7.77 (d, *J* = 6.9, 1H), 7.68 (s, 2H), 7.60–7.46 (m, 4H), 5.36 (s, 2H), 3.03–2.82 (m, 3H), 2.72–2.60 (m, 2H), 2.11–2.01 (m, 1H), 1.76–1.61 (m, 1H); HRMS *m/z* calcd for C<sub>22</sub>H<sub>21</sub>ON<sub>8</sub> [M + H]<sup>+</sup> 413.1833; found 413.1850; SFC retention time 0.96 min. **15'**: <sup>1</sup>H NMR (400 MHz, DMSO) δ 12.89 (s, 1H), 12.57 (s, 1H), 10.14 (s, 1H), 8.17 (s, 1H), 7.77 (d, *J* = 6.9, 1H), 7.68 (s, 2H), 7.60–7.46 (m, 4H), 5.36 (s, 2H), 3.03–2.82 (m, 3H), 2.73–2.57 (m, 2H), 2.12–1.99 (m, 1H), 1.76–1.61 (m, 1H); HRMS *m/z* calcd for C<sub>22</sub>H<sub>21</sub>ON<sub>8</sub> [M + H]<sup>+</sup> 413.1833; found 413.1848; SFC retention time 1.22 min.

*N*-(1-Benzyl-1*H*-pyrazol-4-yl)-6-methyl-4,5,6,7-tetrahydro-1*H*-indazole-3-carboxamide (**16** and **16'**). **6iii** and **12ii** were reacted according to general procedure F to provide racemic **16**. SFC purification (Phenomenex Cellulose-4 (21.2 mm × 150 mm, 5 μm particle size) at 40% MeOH w/0.1%NH<sub>4</sub>OH; 70 mL/min, 100 bar, 40 °C) provided **16** (4% yield) and **16'** (4% yield). **16**: <sup>1</sup>H NMR (400 MHz, DMSO) δ 10.07 (s, 1H), 8.36 (s, 1H), 8.07 (s, 1H), 7.64 (s, 1H), 7.37–7.25 (m, 3H), 7.25–7.20 (m, 2H), 5.27 (s, 2H), 2.87–2.78 (m, 1H), 2.73 (dd, *J* = 15.8, 5.2, 1H), 2.60–2.48 (m, 1H), 2.18 (dd, *J* = 15.9, 9.6, 1H), 1.90–1.73 (m, 2H), 1.38–1.25 (m, 1H), 1.04 (d, *J* = 6.6, 3H); HRMS *m/z* calcd for C<sub>19</sub>H<sub>22</sub>ON<sub>5</sub> [M + H]<sup>+</sup> 336.1819; found 336.1833; SFC retention time 0.49 min. **16b**: <sup>1</sup>H NMR (400 MHz, DMSO) δ 12.79 (s, 1H), 10.07 (s, 1H), 8.07 (s, 1H), 7.64 (s, 1H), 7.37–7.25 (m, 3H), 7.25–7.20 (m, 2H), 5.27 (s, 2H), 2.87–2.77 (m, 1H), 2.73 (dd, *J* = 15.8, 5.2, 1H), 2.61–2.48 (m, 1H), 2.18 (dd, *J* = 15.9, 9.6, 1H), 1.89–1.73 (m, 2H), 1.38–1.24 (m, 1H), 1.04 (d, *J* = 6.6, 3H); HRMS *m/z* calcd for C<sub>19</sub>H<sub>22</sub>ON<sub>5</sub> [M + H]<sup>+</sup> 336.1819; found 336.1832; SFC retention time 0.57 min.

*N*-(1-Benzyl-1*H*-pyrazol-4-yl)-6,6-dimethyl-4,5,6,7-tetrahydro-1*H*-indazole-3-carboxamide (**17**). **6iv** and **12ii** were reacted according to general procedure F to provide **17** in 57% yield. <sup>1</sup>H NMR (400 MHz, DMSO) δ 12.77 (s, 1H), 10.04 (s, 1H), 8.07 (s, 1H), 7.64 (s, 1H), 7.37–7.20 (m, 5H), 5.27 (s, 2H), 2.66 (t, *J* = 6.3, 2H), 2.38 (s, 2H), 1.47 (t, *J* = 6.4, 2H), 0.96 (s, 6H). HRMS *m/z* calcd for C<sub>20</sub>H<sub>24</sub>ON<sub>5</sub> [M + H]<sup>+</sup> 350.1975; found 350.1990.

*N*-(1-Benzyl-1*H*-pyrazol-4-yl)-5,5-dimethyl-4,5,6,7-tetrahydro-1*H*-indazole-3-carboxamide (**18**). **8ii** and **12ii** were reacted according to general procedure F to provide **18** in 38% yield. <sup>1</sup>H NMR (400 MHz, DMSO) δ 12.84 (s, 1H), 10.07 (s, 1H), 8.05 (s, 1H), 7.64 (s, 1H), 7.37–7.26 (m, 3H), 7.25–7.20 (m, 2H), 5.27 (s, 2H), 2.60 (t, *J* = 6.4, 2H), 2.48 (s, 2H), 1.51 (t, *J* = 6.4, 2H), 0.94 (s, 6H). HRMS *m/z* calcd for C<sub>20</sub>H<sub>24</sub>ON<sub>5</sub> [M + H]<sup>+</sup> 350.1975; found 350.1989.

*N*-(1-Benzyl-1*H*-pyrazol-4-yl)-6,6-difluoro-4,5,6,7-tetrahydro-1*H*-indazole-3-carboxamide (**19**). **6v** and **12ii** were reacted according to general procedure F to provide **19** in 19% yield. <sup>1</sup>H NMR (400 MHz, DMSO) δ 13.12 (s, 1H), 10.22 (s, 1H), 8.08 (s, 1H), 7.64 (s, 1H), 7.37–7.26 (m, 3H), 7.26–7.21 (m, 2H), 5.28 (s, 2H), 3.35–3.21 (m, 2H), 2.87 (t, *J* = 6.4, 2H), 2.28–2.14 (m, 2H). HRMS *m/z* calcd for C<sub>18</sub>H<sub>18</sub>ON<sub>5</sub>F<sub>2</sub> [M + H]<sup>+</sup> 358.1474; found 358.1487.

*N*-(1-Benzyl-1*H*-pyrazol-4-yl)-1',4',5',7'-tetrahydrospiro[cyclopropane-1,6'-indazole]-3'-carboxamide (**20**). **6vi** and **12ii** were reacted according to general procedure F to provide **20** in 44% yield. <sup>1</sup>H NMR (400 MHz, DMSO) δ 12.89 (s, 1H), 10.13 (s, 1H), 8.07 (s, 1H), 7.65 (s, 1H), 7.38–7.26 (m, 3H), 7.26–7.21 (m, 2H), 5.28 (s, 2H), 4.38 (d, *J* = 5.7, 2H), 4.27 (d, *J* = 5.7, 2H), 2.99 (s, 2H), 2.69 (t, *J* = 6.3, 2H), 2.03 (t, *J* = 6.3, 2H). HRMS *m/z* calcd for C<sub>20</sub>H<sub>22</sub>ON<sub>5</sub> [M + H]<sup>+</sup> 348.1819; found 348.1832.

*N*-(1-Benzyl-1*H*-pyrazol-4-yl)-6-methoxy-6-methyl-4,5,6,7-tetrahydro-1*H*-indazole-3-carboxamide (**21** and **21'**). **6vii** and **12ii** were reacted according to general procedure F to provide racemic **21**. SFC purification (Lux Cellulose-3 (4.6 mm × 50 mm, 5 μm particle size) at 20% MeOH w/0.1%NH<sub>4</sub>OH; 5 mL/min, 120 bar, 40 °C) provided **21** (21% yield) and **21'** (21% yield). **21**: <sup>1</sup>H NMR (400 MHz, DMSO) δ 12.80 (s, 1H), 10.07 (s, 1H), 8.07 (s, 1H), 7.64 (s, 1H), 7.38–7.19 (m, 5H), 5.27 (s, 2H), 3.13 (s, 3H), 2.78–2.54 (m, 4H), 1.95–1.84 (m, 1H), 1.68–1.57 (m, 1H), 1.22 (s, 3H); HRMS *m/z* calcd for C<sub>20</sub>H<sub>24</sub>O<sub>2</sub>N<sub>5</sub> [M + H]<sup>+</sup> 366.1925; found 366.1941; SFC retention time 0.38 min. **21'**: <sup>1</sup>H NMR (400 MHz, DMSO) δ 12.80 (s, 1H), 10.07 (s, 1H), 8.07 (s, 1H), 7.64 (s, 1H), 7.38–7.20 (m, 5H), 5.27 (s, 2H), 3.13 (s, 3H), 2.77–2.55 (m, 4H), 1.95–1.85 (m, 1H), 1.68–1.57 (m, 1H), 1.22 (s, 3H); HRMS *m/z* calcd for C<sub>20</sub>H<sub>24</sub>O<sub>2</sub>N<sub>5</sub> [M + H]<sup>+</sup> 366.1925; found 366.1938; SFC retention time 0.46 min.

*N*-(1-Benzyl-1*H*-pyrazol-4-yl)-6-(hydroxymethyl)-6-methyl-4,5,6,7-tetrahydro-1*H*-indazole-3-carboxamide (**22** and **22'**). **6viii** and **12ii** were reacted according to general procedure F to provide racemic **22**. SFC purification (Phenomenex Amylose-2 (21.2 mm × 250 mm, 5 μm particle size) at 35% MeOH w/0.1%NH<sub>4</sub>OH; 40 mL/min, 100 bar, 40 °C) provided **22** (24% yield) and **22'** (18% yield). **22**: <sup>1</sup>H NMR (400 MHz, DMSO) δ 12.61 (s, 1H), 10.05 (s, 1H), 8.07 (s, 1H), 7.64 (s, 1H), 7.37–7.25 (m, 3H), 7.25–7.20 (m, 2H), 5.27 (s, 2H), 4.63 (s, 1H), 3.21 (s, 2H), 2.78–2.65 (m, 1H), 2.63–2.48 (m, 2H), 2.26 (d, *J* = 16.0, 1H), 1.59–1.49 (m, 1H), 1.47–1.37 (m, 1H), 0.87 (s, 3H); HRMS *m/z* calcd for C<sub>20</sub>H<sub>24</sub>O<sub>2</sub>N<sub>5</sub> [M + H]<sup>+</sup> 366.1925; found 366.1940; SFC retention time 0.61 min. **22'**: <sup>1</sup>H NMR (400 MHz, DMSO) δ 12.79 (s, 1H), 10.08 (s, 1H), 8.07 (s, 1H), 7.64 (s, 1H), 7.37–7.26 (m, 3H), 7.25–7.20 (m, 2H), 5.27 (s, 2H), 4.62 (t, *J* = 5.4, 1H), 3.21 (d, *J* = 5.4, 2H), 2.72 (dt, *J* = 16.7, 5.6, 1H), 2.63–2.48 (m, 2H), 2.26 (d, *J* = 16.1, 1H), 1.59–1.49 (m, 1H), 1.47–1.37 (m, 1H), 0.87 (s, 3H); HRMS *m/z* calcd for C<sub>20</sub>H<sub>24</sub>O<sub>2</sub>N<sub>5</sub> [M + H]<sup>+</sup> 366.1925; found 366.1939; SFC retention time 0.49 min.

*N*-(1-Benzyl-1*H*-pyrazol-4-yl)-1,4,5,7-tetrahydrospiro[indazole-6,3'-oxetane]-3-carboxamide (**23**). **6ix** and **12ii** were reacted according to general procedure F to provide **23** in 58% yield. <sup>1</sup>H NMR (400 MHz, DMSO) δ 12.93 (s, 1H), 10.10 (s, 1H), 8.07 (s, 1H), 7.64 (s, 1H), 7.37–7.25 (m, 3H), 7.25–7.20 (m, 2H), 5.27 (s, 2H), 4.39 (d, *J* = 5.8, 2H), 4.32 (d, *J* = 5.8, 2H), 2.94 (s, 2H), 2.72 (t, *J* = 6.1, 2H), 1.97 (t, *J* = 6.3, 2H). HRMS *m/z* calcd for C<sub>20</sub>H<sub>22</sub>O<sub>2</sub>N<sub>5</sub> [M + H]<sup>+</sup> 364.1768; found 364.1781.

*N*-(1-Benzyl-1*H*-pyrazol-4-yl)-1',4',4',5',5',7'-hexahydro-2*H*-spiro[*furan*-3,6'-indazole]-3'-carboxamide (**24** and **24'**). **6x** and **12ii** were reacted according to general procedure F to provide racemic **24**. SFC purification (Lux Cellulose-3 (4.6 mm × 50 mm, 5 μm particle size) at 25% MeOH w/0.1%NH<sub>4</sub>OH; 5 mL/min, 120 bar, 40 °C) provided **24** (29% yield) and **24'** (28% yield). **24**: <sup>1</sup>H NMR (400 MHz, DMSO) δ 12.88 (s, 1H), 10.09 (s, 1H), 8.07 (s, 1H), 7.64 (s, 1H), 7.39–7.18 (m, 5H), 5.27 (s, 2H), 3.80 (t, *J* = 7.1 Hz, 2H), 3.48 (d, *J* = 8.4 Hz, 1H), 3.42 (d, *J* = 8.4 Hz, 1H), 2.71 (t, *J* = 6.4 Hz, 2H), 2.61 (s, 2H), 1.82–1.60 (m, 4H); HRMS *m/z* calcd for C<sub>21</sub>H<sub>24</sub>O<sub>2</sub>N<sub>5</sub> [M + H]<sup>+</sup> 378.1925; found 378.1940; SFC retention time 0.36 min. **24'**: <sup>1</sup>H NMR (400 MHz, DMSO) δ 12.85 (s, 1H), 10.09 (s, 1H), 8.07 (s, 1H), 7.64 (s, 1H), 7.37–7.20 (m, 5H), 5.27 (s, 2H), 3.80 (t, *J* = 7.1 Hz, 2H), 3.48 (d, *J* = 8.4 Hz, 1H), 3.42 (d, *J* = 8.4 Hz, 1H), 2.71 (t, *J* = 6.4 Hz, 2H), 2.61 (s, 2H), 1.82–1.60 (m, 4H); HRMS *m/z* calcd for C<sub>21</sub>H<sub>24</sub>O<sub>2</sub>N<sub>5</sub> [M + H]<sup>+</sup> 378.1925; found 378.1940; SFC retention time 0.51 min.

*N*-(1-Benzyl-1*H*-pyrazol-4-yl)-1,4,4a,5,5a,6-hexahydrocyclopropa[*f*]indazole-3-carboxamide (**25** and **25'**). **10xi** and **12ii** were reacted according to general procedure F, omitting step 3 (SEM deprotection), to provide racemic **25**. Preparative chiral HPLC (ChiralPak IC (4.6 mm × 250 mm, 5 μm particle size); eluent = hexane(0.1% Et<sub>3</sub>N):EtOH 80:20; 1.0 mL/min, 5.2 MPA, 25 °C) provided **25** (5.1% yield) and **25'** (3.9% yield). **25**: <sup>1</sup>H NMR (400 MHz, DMSO) δ 12.84 (1H, s), 10.11 (1H, s), 8.09 (1H, s), 7.66 (1H, s), 7.39–7.23 (5H, m), 5.29 (2H, s), 2.70–2.65 (1H, t), 2.36–2.22 (2H, m), 2.13–2.08 (1H, t), 1.73–1.67 (1H, m), 0.91–0.80 (1H, m), 0.50–0.40 (1H, m); HRMS *m/z* calcd for C<sub>19</sub>H<sub>20</sub>ON<sub>5</sub> [M + H]<sup>+</sup> 334.1662; found 334.1676; HPLC retention time 16.23 min. **25'**: <sup>1</sup>H

NMR (400 MHz, DMSO)  $\delta$  12.84 (1H, s), 10.11 (1H, s), 8.09 (1H, s), 7.66 (1H, s), 7.39–7.23 (5H, m), 5.29 (2H, s), 2.70–2.65 (1H, t), 2.36–2.22 (2H, m), 2.13–2.08 (1H, t), 1.73–1.67 (1H, m), 0.91–0.80 (1H, m), 0.50–0.40 (1H, m); HRMS  $m/z$  calcd for  $C_{19}H_{20}ON_5$  [ $M + H$ ]<sup>+</sup> 334.1662; found 334.1678; HPLC retention time 14.26 min.

*N*-(1-Benzyl-1*H*-pyrazol-4-yl)-5*a*-methyl-1,4,4*a*,5,5*a*,6-hexahydrocyclopropa[*f*]indazole-3-carboxamide (**26** and **26'**). **10xii** and **12ii** were reacted according to general procedure F, omitting step 3 (SEM deprotection), to provide racemic **25**. Preparative chiral HPLC (ChiralPak AD-H (4.6 mm  $\times$  150 mm, 5  $\mu$ m particle size); eluent = hexane(0.1% Et<sub>3</sub>N):EtOH 60:40; 1.0 mL/min, 4.4 MPA, 25 °C) provided **26** (13.9% yield) and **26'** (14.4% yield). **26**: <sup>1</sup>H NMR (300 MHz, CDCl<sub>3</sub>, ppm)  $\delta$  8.58 (s, 1H), 8.05 (s, 1H), 7.55 (s, 1H), 7.37–7.32 (m, 3H), 7.30–7.24 (m, 2H), 5.28 (s, 2H), 3.42–3.36 (m, 1H), 3.07–2.97 (m, 2H), 2.74–2.69 (m, 1H), 1.40–1.25 (m, 3H), 1.13–1.07 (m, 1H), 0.42–0.38 (m, 1H), 0.24–0.22 (m, 1H); HRMS  $m/z$  calcd for  $C_{20}H_{22}ON_5$  [ $M + H$ ]<sup>+</sup> 348.1819; found 348.1834; HPLC retention time 9.29 min. **26'**: <sup>1</sup>H NMR (300 MHz, CDCl<sub>3</sub>, ppm)  $\delta$  8.58 (s, 1H), 8.05 (s, 1H), 7.55 (s, 1H), 7.37–7.32 (m, 3H), 7.30–7.24 (m, 2H), 5.28 (s, 2H), 3.42–3.36 (m, 1H), 3.07–2.97 (m, 2H), 2.74–2.69 (m, 1H), 1.40–1.25 (m, 3H), 1.13–1.07 (m, 1H), 0.42–0.38 (m, 1H), 0.24–0.22 (m, 1H); HRMS  $m/z$  calcd for  $C_{20}H_{22}ON_5$  [ $M + H$ ]<sup>+</sup> 348.1819; found 348.1834; HPLC retention time 6.55 min.

(*R*)-*N*-(1-(2-(Dimethylamino)-1-phenylethyl)-1*H*-pyrazol-4-yl)-6,6-dimethyl-4,5,6,7-tetrahydro-1*H*-indazole-3-carboxamide (**27**). **6iv** and **12iii** were reacted according to general procedure F to provide racemic **27**. SFC purification (Chiralpak AD (4.6 mm  $\times$  50 mm, 5  $\mu$ m particle size) at 35% MeOH w/0.1%NH<sub>4</sub>OH; 5 mL/min, 120 bar, 40 °C) provided **27** (9% yield). <sup>1</sup>H NMR (400 MHz, DMSO)  $\delta$  12.91–12.72 (s, 1H), 10.20–9.97 (s, 1H), 8.17–8.15 (s, 1H), 7.64–7.61 (s, 1H), 7.38–7.23 (m, 5H), 5.68–5.46 (dd,  $J = 9.1$ , 5.8 Hz, 1H), 3.28–3.19 (dd,  $J = 12.7$ , 9.4 Hz, 1H), 2.82–2.74 (dd,  $J = 12.9$ , 5.7 Hz, 1H), 2.70–2.63 (t,  $J = 6.3$  Hz, 2H), 2.42–2.37 (s, 2H), 2.21–2.16 (s, 6H), 1.50–1.44 (t,  $J = 6.3$  Hz, 2H), 0.99–0.93 (s, 6H); HRMS  $m/z$  calcd for  $C_{23}H_{31}ON_6$  [ $M + H$ ]<sup>+</sup> 407.2554; found 407.2569; SFC retention time 0.58 min (undesired isomer, 0.43 min).

(*S*)-*N*-(1-(3-(Dimethylamino)-1-phenylpropyl)-1*H*-pyrazol-4-yl)-6,6-dimethyl-4,5,6,7-tetrahydro-1*H*-indazole-3-carboxamide (**28**) and (*R*)-*N*-(1-(3-(Dimethylamino)-1-phenylpropyl)-1*H*-pyrazol-4-yl)-6,6-dimethyl-4,5,6,7-tetrahydro-1*H*-indazole-3-carboxamide (**28'**). **6iv** and **12iv** were reacted according to general procedure F to provide racemic **28**. SFC purification (Phenomenex Cellulose-4 (21.2 mm  $\times$  150 mm, 5  $\mu$ m particle size) at 45% MeOH w/0.1%NH<sub>4</sub>OH; 70 mL/min, 100 bar, 40 °C) provided **28** (21% yield) and **28'** (24% yield). **28**: <sup>1</sup>H NMR (400 MHz, DMSO)  $\delta$  12.78 (s, 1H), 10.05 (s, 1H), 8.08 (s, 1H), 7.66 (s, 1H), 7.37–7.22 (m, 5H), 5.42 (dd,  $J = 9.3$ , 5.3, 1H), 2.66 (t,  $J = 6.0$ , 2H), 2.38 (s, 2H), 2.25–2.02 (m, 10H), 1.47 (t,  $J = 6.4$ , 2H), 0.96 (s, 6H); HRMS  $m/z$  calcd for  $C_{24}H_{33}ON_6$  [ $M + H$ ]<sup>+</sup> 421.2710; found 421.2726; SFC retention time 0.37 min. **28'**: <sup>1</sup>H NMR (400 MHz, DMSO)  $\delta$  12.78 (s, 1H), 10.04 (s, 1H), 8.08 (s, 1H), 7.66 (s, 1H), 7.36–7.23 (m, 5H), 5.42 (dd,  $J = 9.2$ , 5.6, 1H), 2.66 (t,  $J = 6.2$ , 2H), 2.38 (s, 2H), 2.23–2.00 (m, 10H), 1.47 (t,  $J = 6.3$ , 2H), 0.96 (s, 6H); HRMS  $m/z$  calcd for  $C_{24}H_{33}ON_6$  [ $M + H$ ]<sup>+</sup> 421.2710; found 421.2729; SFC retention time 0.59 min.

(*S*)-6,6-Dimethyl-*N*-(1-(phenylpiperidin-4-yl)methyl)-1*H*-pyrazol-4-yl)-4,5,6,7-tetrahydro-1*H*-indazole-3-carboxamide (**29**). **6iv** and **12v** were reacted according to general procedure F to provide racemic **29**. SFC purification (Lux Cellulose-1 (4.6 mm  $\times$  50 mm, 5  $\mu$ m particle size) at 30% MeOH w/0.1%NH<sub>4</sub>OH; 5 mL/min, 120 bar, 40 °C) provided **29** (5% yield). <sup>1</sup>H NMR (400 MHz, DMSO)  $\delta$  12.82 (s, 1H), 10.06 (s, 1H), 8.14 (s, 1H), 7.63 (s, 1H), 7.55–7.48 (m, 2H), 7.37–7.30 (m, 2H), 7.30–7.24 (m, 1H), 5.00 (d,  $J = 10.7$  Hz, 1H), 2.97–2.84 (m, 2H), 2.70–2.62 (m, 2H), 2.55–2.36 (m, 6H), 1.46 (t,  $J = 6.3$  Hz, 2H), 1.21–1.00 (m, 4H), 0.96 (s, 6H). HRMS  $m/z$  calcd for  $C_{23}H_{33}ON_6$  [ $M + H$ ]<sup>+</sup> 433.2710; found 433.2723; SFC retention time 0.43 min (undesired isomer: 0.58 min).

(*S*)-6,6-Dimethyl-*N*-(1-(3-(methylsulfonyl)-1-phenylpropyl)-1*H*-pyrazol-4-yl)-4,5,6,7-tetrahydro-1*H*-indazole-3-carboxamide (**30**). **6iv** and **12vi** were reacted according to general procedure F to provide racemic **30**. Preparative chiral HPLC (ChiralPak IB (4.6 mm

$\times$  250 mm, 5  $\mu$ m particle size); eluent = hexane(0.1% Et<sub>3</sub>N):EtOH 80:20; 1.0 mL/min, 5.0 MPA, 25 °C) provided **30** (18% yield). <sup>1</sup>H NMR (300 MHz, CD<sub>3</sub>OD)  $\delta$  8.08 (s, 1H), 7.7 (s, 1H), 7.37–7.26 (m, 5H), 5.55–5.50 (m, 1H), 3.29–2.83 (m, 6H), 2.80–2.72 (m, 2H), 2.67–2.59 (m, 1H), 2.40 (s, 2H), 1.55–1.50 (t,  $J = 6.3$ , 2H), 0.99 (s, 6H). HRMS  $m/z$  calcd for  $C_{23}H_{30}O_3N_8S$  [ $M + H$ ]<sup>+</sup> 456.2064; found 456.2080. HPLC retention time 16.70 min (undesired isomer: 20.43 min).

(*S*)-*N*-(1-(3-(Dimethylamino)-1-(*m*-tolyl)propyl)-1*H*-pyrazol-4-yl)-6,6-dimethyl-4,5,6,7-tetrahydro-1*H*-indazole-3-carboxamide (**31**). **6iv** and **12vii** were reacted according to general procedure F to provide racemic **31**. Preparative chiral HPLC (Venusil chiral OD-H (4.6 mm  $\times$  250 mm, 5  $\mu$ m particle size); eluent = hexane(0.1% Et<sub>3</sub>N):EtOH 90:10; 1.0 mL/min, 3.3 MPA, 25 °C) provided **31** (15% yield). <sup>1</sup>H NMR (300 MHz, CD<sub>3</sub>OD)  $\delta$  8.10 (s, 1H), 7.70 (s, 1H), 7.27–7.11 (m, 4H), 5.40–5.35 (m, 1H), 2.81–2.77 (t,  $J = 12.3$ , 2H), 2.64–2.61 (m, 1H), 2.57 (s, 5H), 2.54 (s, 7H), 1.59–1.32 (m, 2H), 1.04 (s, 6H). MS:  $m/z = 435$  ( $M + H$ ) (insufficient material for HRMS analysis). HPLC retention time 14.10 min (undesired isomer: 21.73 min).

(*S*)-*N*-(1-(1-(3-Chlorophenyl)-3-(dimethylamino)propyl)-1*H*-pyrazol-4-yl)-6,6-dimethyl-4,5,6,7-tetrahydro-1*H*-indazole-3-carboxamide (**32**). **6iv** and **12viii** were reacted according to general procedure F to provide racemic **32**. Preparative chiral HPLC (Venusil chiral OD-H (4.6 mm  $\times$  250 mm, 5  $\mu$ m particle size); eluent = hexane(0.1% Et<sub>3</sub>N):EtOH 90:10; 1.0 mL/min, 3.3 MPA, 25 °C) provided **32** (12% yield). <sup>1</sup>H NMR (300MHz, CD<sub>3</sub>OD, ppm)  $\delta$  8.13 (s, 1H), 7.74 (s, 1H), 7.38–7.28 (m, 4H), 5.47–5.42 (m, 1H), 2.81–2.77 (t,  $J = 12.6$ , 2H), 2.69–2.61 (m, 1H), 2.58 (s, 1H), 2.44–2.35 (m, 2H), 2.34 (s, 9H), 1.59–1.55 (t,  $J = 12.9$ , 2H), 1.04 (s, 6H). HRMS  $m/z$  calcd for  $C_{24}H_{32}ON_6Cl$  [ $M + H$ ]<sup>+</sup> 455.2321; found 455.2341. HPLC retention time 13.35 min (undesired isomer: 17.71 min).

**Pharmaceutical and Biological Assay Protocols. Measured log  $D_{7.4}$ .** Two buffers were used in the assay: a saturated 1-octanol/phosphate buffer solution (20 mL of PBS pH 7.4 + 200 mL of 1-octanol) and a saturated PBS/1-octanol solution (1 mL of 1-octanol + 200 mL of PBS pH 7.4). Each solution was freshly prepared, shaken for 1 h, and allowed to stand for 24 h before use. Saturated 1-octanol/PBS solution (250  $\mu$ L) was dispensed into each well of a 96-deep well plate and followed by 5  $\mu$ L of a 10 mM test compound in DMSO stock solution. The plates were sealed with aluminum sealing film and shaken for 20 min at 1000 rpm. After shaking, 250  $\mu$ L of saturated PBS/1-octanol solution was added to each well. The plates were then resealed, shaken for 1 h at 1000 rpm at room temperature, and centrifuged at 3000 rpm for 10 min. Sample analyses were carried out by transferring the octanol and PBS phases to 384-well plates, with 2  $\mu$ L of 0.1 mM propranolol in acetonitrile solution added to each well as an internal standard. A UPLC/MS/MS equipped with Shimadzu LC and Sciex API4000 was used for quantification of octanol and PBS samples. The quantification was performed by MRM (multiple reaction monitor) transition analysis. With separate injections, 3  $\mu$ L for the octanol samples and 10  $\mu$ L for the PBS samples, MRM peaks were collected, processed, and integrated. The log  $D_{7.4}$  of the compound was determined as the log of the ratio of MRM peaks in octanol and PBS phases.

**Kinetic Solubility.** Kinetic solubility in PBS buffer at pH 7.4 was determined using 10 mM DMSO stock solutions for each compound. 96-well Millipore filtration plates were used for this assay with each well containing 196  $\mu$ L of PBS buffer solution and 4  $\mu$ L of DMSO stock solution. The filter plate was sealed with aluminum sealing film and was shaken for 24 h at 1000 rpm at room temperature. The incubation solution was then filtered into a clean 96-well plate using a vacuum manifold and diluted by 2 and 4 times (two different dilutions used for internal quality control) with PBS/MeOH(1/1 v/v) mixture. An Agilent 1290 HPLC and equipped with an Antek 8060 CLND was used for solubility quantitation. The CLND was calibrated using caffeine in a H<sub>2</sub>O/MeOH (1/1 v/v) solution as a standard at eight different concentrations from 2 to 4500  $\mu$ M. Then 5  $\mu$ L of each sample was injected onto a reverse phase C18 column and a 4 min LC gradient from 98:2 to 2:98 A:B (A = 0.1% TFA in H<sub>2</sub>O; B = 0.1% TFA

in MeOH) at a flow rate of 400  $\mu\text{L}/\text{min}$  was used. The solubility was determined by nitrogen response of CLND.

**ITK Biochemical Assay.** GST-ITK full-length enzyme was from Invitrogen (PV3875) and the substrate was BLK peptide (Ac-EFPIYDFLPAKKK-NH<sub>2</sub>). Reactions were carried out in a final volume of 51  $\mu\text{L}$  with 50 mM HEPES (pH 7.2), 15 mM MgCl<sub>2</sub>, 2 mM DTT, 0.015% Brij-35, 1 nM ITK, 2  $\mu\text{M}$  substrate, 20  $\mu\text{M}$  ATP, and test article in a final concentration of 2% DMSO. After 35 min incubation at rt, reactions were stopped upon addition of 10  $\mu\text{L}$  of 30% TCA. Samples were centrifuged (4350 rpm, 4 °C, 5 min) and subjected to LC/MS analysis on a Waters Acquity UPLC/TQD system equipped with a Waters Acquity UPLC BEH C18 (2.1 mm  $\times$  50 mm) 1.7  $\mu\text{m}$  column (injection volume, 5  $\mu\text{L}$ ; column temperature, 60 °C; flow rate, 1 mL/min; solvent A, 0.1% formic acid in LC/MS grade water; solvent B, 0.1% formic acid in LC/MS grade ACN). Analytes were separated by applying a gradient from 15% to 32% solvent B within 0.7 min and detected in positive mode ESI-MS/MS by MRM (multiple reaction monitoring) of transitions 819.8/84.8 (BLK substrate) and 859.0/84.8 as well as 859.0/120.7 (phosphorylated BLK product).  $K_i$  values were determined using the Morrison tight-binding model<sup>31</sup> modified to account for an ATP-competitive mechanism of inhibition and for the concentration of active kinase used (0.3 nM ITK). Using this approach, the lower limit of  $K_i$  measurable is approximately 250-fold lower than the ITK concentration, or 0.0012 nM.

**Aurora A Biochemical Assay.** HIS-tagged human AURKA full length enzyme was purchased either from Invitrogen (PV3612) or from Millipore (14–511), and substrate was a generic Kemptide peptide (Ac-LRRASLG-NH<sub>2</sub>). Reactions were carried out in a final volume of 51  $\mu\text{L}$  with 50 mM HEPES (pH 7.2), 10 mM MgCl<sub>2</sub>, 2 mM DTT, 0.015% Brij-35, 10 nM AURKA, 2  $\mu\text{M}$  substrate, 100  $\mu\text{M}$  ATP, and 2% DMSO. After 60 min incubation at RT, reactions were stopped upon addition of 10  $\mu\text{L}$  of 30% TCA. Samples were centrifuged (4350 rpm, 4 °C, 5 min) and subjected to LC/MS analysis on a Waters Acquity UPLC/TQD system equipped with a Waters Acquity UPLC BEH C18 (2.1 mm  $\times$  50 mm) 1.7  $\mu\text{m}$  column (injection volume, 5  $\mu\text{L}$ ; column temperature, 60 °C; flow rate, 1 mL/min; solvent A, 0.1% formic acid in LC/MS grade water; solvent B, 0.1% formic acid in LC/MS grade ACN). Analytes were separated by applying a gradient from 10 to 13% solvent B within 0.7 min and detected in positive mode ESI-MS/MS by MRM (multiple reaction monitoring) of transitions 813.3/86.2 (Kemptide substrate) and 893.3/86.2 as well as 893.3/795.5 (phosphorylated Kemptide product).  $K_i$  values were calculated as above for the ITK assay.

**PLC $\gamma$  Cellular Assay.** Jurkat T-cells (400 K cells/well) were suspended in assay buffer (D-PBS + 0.1% glucose + 10% FBS + 0.22  $\mu\text{M}$  sodium pyruvate), seeded in 96-well plate, treated with compounds for 30 min, and stimulated with anti-CD3 Dynabeads (Invitrogen,  $4 \times 10^6$  beads/well) for 2 min at 37 °C. The cells were pelleted by brief spinning, and after aspirating off media, 30  $\mu\text{L}$  of 1 $\times$  lysis buffer (Cell Signaling Technology) was added to each well, and the plate was incubated at 4 °C for 30 min while shaking. After beads were quickly spun down, 25  $\mu\text{L}$  of lysate from each well was transferred to capture antibody (mouse monoclonal antibody to human PLC $\gamma$ 1, from Abcam) coated MSD goat antimouse 96-well plate (MesoScale Discovery) and incubated at 4 °C overnight with shaking. After washing four times with 150  $\mu\text{L}$  of MSD Tris buffer (50 mM Tris-HCl, pH 7.5, 150 mM NaCl, 0.02% Tween-20), 25  $\mu\text{L}$  of detection antibodies (1:2000 dilution mixture of rabbit anti-pPLC $\gamma$ 1, from Cell Signaling Technology and goat antirabbit SULFO-Tag from MesoScale Discovery) were added and incubated for 2 h at room temperature. After washing of plate four times with 150  $\mu\text{L}$  of MSD Tris buffer, 150  $\mu\text{L}$  of 1 $\times$  MSD read buffer T was added to each well, and the plate was read out on SECTOR Imager 6000 (MesoScale Discovery).

## ■ ASSOCIATED CONTENT

### ● Supporting Information

Procedures for the synthesis of ketones 4ii,viii–x, and 9xii; crystallographic method, data refinement and statistics for all disclosed crystal structures; full kinase selectivity panel for 28. This material is available free of charge via the Internet at <http://pubs.acs.org>.

### Accession Codes

The PDB ID code for 2 bound to Aurora-A is 4PRJ; the ID code for 28 bound to ITK is 4PQN.

## ■ AUTHOR INFORMATION

### Corresponding Author

\*Phone: 650-467-6059. E-mail: [burch.jason@gene.com](mailto:burch.jason@gene.com).

### Author Contributions

The manuscript was written through contributions of all authors. All authors have given approval to the final version of the manuscript.

### Notes

The authors declare no competing financial interest.

## ■ ACKNOWLEDGMENTS

We thank Deven Wang for HRMS measurements, Dr. Baiwei Lin for kinetic solubility and log *D* measurements, Chris Hamman, Mengling Wong, and Michael Hayes for compound purification, Allan Jaochico, Xiao Ding, and Justin Ly for in vivo PK data, and Connie Chan for formulation work. Drs. Matthew Volgraf, James Crawford, and Steven Staben are gratefully acknowledged for their careful editing of this manuscript.

## ■ ABBREVIATIONS USED

ACN, acetonitrile; ADME, absorption–distribution–metabolism–elimination; AUC, area under the curve; ATP, adenine triphosphate; Aur-A, Aurora A; Cl, clearance; CLND, chemiluminescence nitrogen detector; DEAD, diethyl azodicarboxylate; %*F*, bioavailability (fraction absorbed); HEPES, 4-(2-hydroxyethyl)-1-piperazineethanesulfonic acid; HPLC, high-pressure liquid chromatography; hPPB, human plasma protein binding; HTS, high-throughput screen; IL, interleukin; ITK, interleukin-2 inducible T-cell kinase; LDA, lithium diisopropylamide; LE, ligand efficiency; mCPBA, *meta*-chloroperbenzoic acid; MDCK, Madin–Darby canine kidney; MOE, Molecular Operating Environment; MRM, multiple reaction monitoring; NMP, *N*-methyl pyrrolidone; PBS, phosphate buffer solution; PLC $\gamma$ , phosphoinositide phospholipase C gamma; pyr, pyridine; rt, room temperature; SAR, structure–activity relationships; SEDDS, self-emulsifying drug delivery system; SEM, 2-(trimethylsilyl)ethoxymethyl; SFC, supercritical fluid chromatography; SFI, solubility forecast index;  $T_{1/2}$ , half-life; TBTU, *O*-(benzotriazol-1-yl)-*N,N,N',N'*-tetramethyluronium tetrafluoroborate; TCA, trichloroacetic acid; TCR, T-cell receptor; TFA, trifluoroacetic acid; THI, tetrahydroindazole; THF, tetrahydrofuran; TPSA, topological polar surface area; Vss, volume of distribution at steady state

## ■ REFERENCES

- (1) (a) Berg, L. J.; Finkelstein, L. D.; Lucas, J. A.; Schwartzberg, P. L. Tec family kinases in T lymphocyte development and function. *Annu. Rev. Immunol.* **2005**, *23*, 549–600. (b) Felices, M.; Falk, M.; Kosaka, Y.; Berg, L. J. Tec kinases in T Cell and Mast Cell Signaling. *Adv. Immunol.* **2007**, *93*, 145–184.

- (2) (a) Liu, K. Q.; Bunnell, S. C.; Gurniak, C. B.; Berg, L. J. T cell receptor-initiated calcium release is uncoupled from capacitative calcium entry in Itk-deficient T cells. *J. Exp. Med.* **1998**, *187*, 1721–1727. (b) Schaeffer, E. M.; Debnath, J.; Yap, G.; McVicar, D.; Liao, X. C.; Littman, D. R.; Sher, A.; Varmus, H. E.; Lenardo, M. J.; Schwartzberg, P. L. Requirement for Tec kinases Rlk and Itk in T cell receptor signaling and immunity. *Science* **1999**, *284*, 638–641. (c) Ellmeier, W.; Jung, S.; Sunshine, M. J.; Hatam, F.; Xu, Y.; Baltimore, D.; Mano, H.; Littman, D. R. Severe B cell deficiency in mice lacking the Tec kinase family members Tec and Btk. *J. Exp. Med.* **2000**, *192*, 1611–1624.
- (3) (a) Liao, X. C.; Littman, D. R. Altered T cell receptor signaling and disrupted T cell development in mice lacking Itk. *Immunity* **1995**, *3*, 757–769. (b) Fowell, D. J.; Shinkai, K.; Liao, X. C.; Beebe, A. M.; Coffman, R. L.; Littman, D. R.; Locksley, R. M. Impaired NFATc translocation and failure of Th2 development in Itk-deficient CD4+ T cells. *Immunity* **1999**, *11*, 399–409. (c) Schaeffer, E. M.; Yap, G. S.; Lewis, C. M.; Czar, M. J.; McVicar, D. W.; Cheever, A. W.; Sher, A.; Schwartzberg, P. L. Mutation of Tec family kinases alters T helper cell differentiation. *Nature Immunol.* **2001**, *2*, 1183–1188.
- (4) Mueller, C.; August, A. Attenuation of immunological symptoms of allergic asthma in mice lacking the tyrosine kinase ITK. *J. Immunol.* **2003**, *170*, 5056–5063.
- (5) (a) Das, J.; Liu, C.; Moquin, R. V.; Lin, J.; Furch, J. A.; Spergel, S. H.; McIntyre, K. W.; Shuster, D. J.; O'Day, K. D.; Penhallow, B.; Huang, C.-Y.; Kanner, S. B.; Lin, T.-A.; Dodd, J. H.; Barrish, J. C.; Wityak, J. Discovery and SAR of 2-amino-5-[(thiomethyl)aryl]-thiazoles as potent and selective Itk inhibitors. *Bioorg. Med. Chem. Lett.* **2006**, *16*, 2411–2415. (b) Lin, T. A.; McIntyre, K.; Das, J.; Liu, C.; O'Day, K. D.; Penhallow, C.-Y.; Whitney, G. S.; Shuster, D. J.; Xia, X.; Townsend, R.; Postelnek, J.; Spergel, S. H.; Lin, J.; Moquin, R. V.; Furch, J. A.; Kamath, A. V.; Zhang, H.; Marathe, P. H.; Perez-Villar, J. J.; Doweiko, A.; Killar, L.; Dodd, J. H.; Barrish, J. C.; Wityak, J.; Kanner, S. B. Selective Itk inhibitors block T-cell activation and murine lung inflammation. *Biochemistry* **2004**, *43*, 11056–11062. (c) Snow, R. J.; Abeywardane, A.; Campbell, S.; Lord, J.; Kashem, M. A.; Khine, H. H.; King, J.; Kowalski, J. A.; Pullen, S. S.; Roma, T.; Roth, G. P.; Sarko, C. R.; Wilson, N. S.; Winter, M. P.; Wolak, J. P.; Cywin, C. L. Hit-to-lead studies on benzimidazole inhibitors of ITK: discovery of a novel class of kinase inhibitors. *Bioorg. Med. Chem. Lett.* **2007**, *17*, 3660–3665. (d) Moriarty, K. J.; Winters, M.; Qiao, L.; Ryan, D.; DesJarlis, R.; Robinson, D.; Cook, B. N.; Kashen, M. A.; Kaplita, P. V.; Liu, L. H.; Farrell, T. M.; Khine, H. H.; King, J.; Pullen, S. S.; Roth, G. P.; Magolda, R.; Takahashi, H. Itk kinase inhibitors: Initial efforts to improve the metabolic stability and the cell activity of the benzimidazole lead. *Bioorg. Med. Chem. Lett.* **2008**, *18*, 5537–5540. (e) Winters, M. P.; Robinson, D. J.; Khine, H. H.; Pullen, S. S.; Woska, J. R., Jr.; Raymond, E. L.; Sellati, R.; Cywin, C. L.; Snow, R. J.; Kashem, M. A.; Wolak, J. P.; King, J.; Kaplita, P. V.; Liu, L. H. 5-Aminomethyl-1H-benzimidazoles as orally active inhibitors of inducible T-cell kinase (Itk). *Bioorg. Med. Chem. Lett.* **2008**, *18*, 5541–5544. (f) Moriarty, K. J.; Takahashi, H.; Pullen, S. S.; Khine, H. H.; Sallati, R. H.; Raymond, E. L.; Woska, J. R., Jr.; Jeanfavre, D. D.; Roth, G. P.; Winters, M. P.; Qiao, L.; Ryan, D.; DesJarlais, R.; Robinson, D.; Wilson, M.; Bobko, M.; Cook, B. N.; Lo, H. Y.; Nemoto, P. A.; Kashen, M. A.; Wolak, J. P.; White, A.; Magolda, R. L.; Tomczuk, B. Discovery, SAR and X-ray structure of 1H-benzimidazole-5-carboxylic acid cyclohexyl-methylamides as inhibitors of inducible T-cell kinase (Itk). *Bioorg. Med. Chem. Lett.* **2008**, *18*, 5545–5549. (g) Riether, D.; Zindell, R.; Kowalski, J. A.; Cook, B. N.; Bentzien, J.; De Lombaert, S.; Thomson, D.; Kugler, S. Z., Jr.; Skow, D.; Martin, L. S.; Raymond, E. L.; Khine, H. H.; O'Shea, K.; Woska, J. R., Jr.; Jeanfavre, D.; Sellati, R.; Ralph, K. L. M.; Ahlberg, J.; Labissiere, G.; Kashem, M. A.; Pullen, S. S.; Takahashi, H. 5-Aminomethylbenzimidazoles as potent ITK antagonists. *Bioorg. Med. Chem. Lett.* **2009**, *19*, 1588–1591. (h) Lo, H. Y.; Bentzien, J.; Fleck, R. W.; Pullen, S. S.; Khine, H. H.; Woska, J. R.; Kugler, S. Z.; Kashen, M. A.; Takahashi, H. 2-Aminobenzimidazoles as potent ITK antagonists: trans-stilbene-like moieties targeting the kinase specificity pocket. *Bioorg. Med. Chem. Lett.* **2008**, *18*, 6218–6221. (i) Charrier, J. D.; Miller, A.; Kay, D. P.; Brenchley, G.; Twin, H. C.; Collier, P. N.; Ramaya, S.; Keily, S. B.; Durrant, S. J.; Knechtel, R. M.; Tanner, A. J.; Brown, K.; Curnock, A. P.; Jimenez, J. M. Discovery and structure-activity relationships of 3-aminopyrid-2-ones as potent and selective interleukin-2 inducible T-cell kinase (Itk) inhibitors. *J. Med. Chem.* **2011**, *54*, 2341–2350. (j) Herdemann, M.; Weber, A.; Jonveaux, J.; Jonveaux, J.; Schwoebel, S.; Heit, I. Optimization of ITK inhibitors through successive design cycles. *Bioorg. Med. Chem. Lett.* **2011**, *21*, 1852–1856. (k) McLean, L. R.; Zhang, Y.; Zaidi, N.; Bi, X.; Wang, R.; Dharanipragada, R.; Jurcak, J. G.; Gillespy, T. A.; Zhao, Z.; Musick, K. Y.; Choi, Y. M.; Barrague, M.; Peppard, J.; Smicker, M.; Duguid, M.; Parkar, A.; Fordham, J.; Kominos, D. X-ray crystallographic structure-based design of selective thienopyrazole inhibitors of interleukin-2-inducible tyrosine kinase. *Bioorg. Med. Chem. Lett.* **2012**, *22*, 3296–3300. (l) Zapf, C. W.; Gerstenberger, B. S.; Xing, L.; Limburg, D. C.; Anderson, D. R.; Caspers, N.; Han, S.; Aulabaugh, A.; Kurumbail, R.; Shakya, S.; Li, X.; Spaulding, V.; Czerwinski, R. M.; Seth, N.; Medley, Q. G. Covalent inhibitors of interleukin-2 inducible T cell kinase (Itk) with nanomolar potency in a whole blood assay. *J. Med. Chem.* **2012**, *55*, 10047–10063. (m) Pastor, R. M.; Burch, J. D.; Magnuson, S.; Ortwine, D. O.; Chen, Y.; De La Torre, K.; Ding, X.; Eigenbrot, C.; Johnson, A.; Liimatta, A.; Liu, Y.; Shia, S.; Wang, X.; Wu, L. C.; Pei, Z. Discovery and optimization of indazoles as potent and selective interleukin-2 inducible T cell kinase (ITK) inhibitors. *Bioorg. Med. Chem. Lett.* **2014**, *24*, 2448–2452. (n) Harling, D. J.; Deakin, A. M.; Campos, S.; Grimley, R.; Chaudry, L.; Nye, C.; Polyakova, O.; Bessant, C. M.; Barton, N.; Somers, D.; Barrett, J.; Graves, R. H.; Hanns, L.; Kerr, W. J.; Solari, R. Discovery of Novel Irreversible Inhibitors of Interleukin (IL)-2-inducible tyrosine kinase (Itk) by targeting cysteine 442 in the ATP pocket. *J. Biol. Chem.* **2013**, *288*, 28195–28206. (o) Alder, C. M.; Ambler, M.; Campbell, A. J.; Champigny, A. C.; Deakin, A. M.; Harling, J. D.; Harris, C. A.; Longstaff, T.; Lynn, S.; Maxwell, A. C.; Mooney, C. J.; Scullion, C.; Singh, O. M. P.; Smith, I. E. D.; Somers, D. O.; Tame, C. J.; Wayne, G.; Wilson, C.; Woolven, J. M. Identification of a novel and selective series of Itk inhibitors via a template-hopping strategy. *ACS Med. Chem. Lett.* **2013**, *4*, 948–952. For a recent review on ITK inhibitors, see: (p) Charrier, J.-D.; Knechtel, R. M. Advances in the design of ITK inhibitors. *Expert Opin. Drug Discovery* **2013**, *8*, 369.
- (6) The cellular potency of inhibitor **3** reported here differs slightly from that reported previously ( $IC_{50} = 173$  nM reported in ref 5m) because the assay conditions were varied to include 10% FBS. For more details, see the Experimental Section.
- (7) For syntheses of ketones not previously disclosed in the chemical literature (**4ii**, **4viii**, and **4x** and **9xii**) please refer to the Supporting Information.
- (8) Royals, E. E. The use of sodium methoxide in the Claisen reaction. *J. Am. Chem. Soc.* **1945**, *67*, 1508–1509.
- (9) Padwa, A.; Kulkarni, Y. S.; Zhang, Z. Reaction of carbonyl compounds with ethyl lithiodiazoacetate. Studies dealing with rhodium(II)-catalyzed behavior of the resulting adducts. *J. Org. Chem.* **1990**, *55*, 4144–4153.
- (10) Following the completion of our work, an elegant one-pot conversion of ketones and diazoacetates to pyrazole carboxylic esters was reported which results in the desired regiochemical outcome: Wang, L.; Huang, J.; Gong, X.; Wang, J. Highly regioselective organocatalyzed synthesis of pyrazoles from diazoacetates and carbonyl compounds. *Chem.—Eur. J.* **2013**, *19*, 7555–7560.
- (11) (a) Mitsunobu, O. The use of diethyl azodicarboxylate and triphenylphosphine in synthesis and transformation of natural products. *Synthesis* **1981**, 1–28. (b) Zabierek, A. A.; Konrad, K. M.; Haidle, A. M. A practical two-step synthesis of 1-alkyl-4-aminopyrazoles. *Tetrahedron Lett.* **2008**, *49*, 2996–2998.
- (12) Manning, G.; Whyte, D. B.; Martinez, R.; Hunter, T.; Sudarsanam, S. The protein kinase complement of the human genome. *Science* **2002**, *298*, 1912–1934.
- (13) Figure was created using MOE (www.chemcomp.com).
- (14) Bolanos-Garcia, V. M. Aurora kinases. *Int. J. Biochem. Cell. Biol.* **2005**, *37*, 1572–2577.

- (15) Hill, A. P.; Young, R. J. Getting physical in drug discovery: a contemporary perspective on solubility and hydrophobicity. *Drug Discovery Today* **2010**, *15*, 648–655.
- (16) cLogD<sub>7.4</sub> was calculated using v1.1 of MoKa, available from Molecular Discovery Ltd. ([www.moldiscovery.com](http://www.moldiscovery.com)).
- (17) Belanger, D. B.; Curran, P. J.; Hruza, A.; Voigt, J.; Meng, Z.; Mandal, A. K.; Siddiqui, M. A.; Basso, A. D.; Gray, K. Discovery of imidazo[1,2-*a*]pyrazine-based Aurora kinase inhibitors. *Bioorg. Med. Chem. Lett.* **2010**, *20*, 5170–5174.
- (18) External ITK structures available in the Protein Data Bank (PDB) were loaded into MOE ([www.chemcomp.com](http://www.chemcomp.com)) and solvent-accessible surface representations of the active site were generated. For external structures, see refs 5i, 5k, 5l, 5n, and 5o as well as: Kutach, A. K.; Villasenor, A. G.; Lam, D.; Belunis, C.; Janson, C.; Lok, S.; Hong, L.-N.; Liu, C.-M.; Deval, J.; Novak, T. J.; Barnett, J. W.; Chu, W.; Shaw, D.; Kuglstatter, A. Crystal structures of IL-2-inducible T cell kinase complexed with inhibitors: insights into rational drug design and activity regulation. *Chem. Biol. Drug Des.* **2010**, *76*, 154–163.
- (19) Concurrent with our investigations, a related but distinct series of tetrahydroindazole-containing ITK inhibitors appeared in the patent literature, which also feature 6,6-dimethylation in the majority of the examples: Inoue, T.; Kaya, T.; Kikuchi, S.; Matsumura, K.; Masuo, R.; Suzuki, M.; Maekawa, M. Indole compounds and pharmaceutical use thereof. US2011/0306599 A1, 2011.
- (20) Differences in plasma protein binding can also not explain the differences in cell shift, as the cellular assay has a low serum content (10% FBS), and the compounds have similar hPPB (17, 98%; 27, 95%; 28, 93%).
- (21) CLK2 (93%), Flt3 (76%), Flt3(D835Y) (75%), TrkA (80%), TrkB (91%), TrkC (88%). ITK reference: 98%. For the full list of kinases and inhibitions, refer to the Supporting Information.
- (22) Self-emulsifying drug delivery systems (SEDDS), which are mixtures of oils, surfactants and solvents, have been shown to be beneficial for the oral absorption and/or solubilization of lipophilic drugs. For a review see: Gursoy, R. N.; Benita, S. Self-emulsifying drug delivery systems (SEDDS) for improved oral delivery of lipophilic drugs. *Biomed. Pharmacother.* **2004**, *58*, 173–182.
- (23) Kuntz, D. I.; Chen, K.; Sharp, K. A.; Kollman, P. A. The maximal affinity of ligands. *Proc. Natl. Acad. Sci. U. S. A.* **1999**, *96*, 9997–10002.
- (24) Wulff, W. D.; Su, J.; Tang, P.-C.; Xu, Y.-C. Studies toward the synthesis of menogaril: synthesis of A-ring precursors and their conversion to the tetracyclic core via the benzannulation reaction. *Synthesis* **1999**, 415–422.
- (25) Chan, J. H.-H.; Rickborn, B. Relative rates and stereochemistry of the iodozincmethyl iodide methylenation of some hydroxyl- and methoxy-substituted cyclic olefins. *J. Am. Chem. Soc.* **1968**, *90*, 6406–6411.
- (26) Miyano, S.; Lu, L. D.-L.; Viti, S. M.; Sharpless, K. B. Kinetic resolution of racemic  $\beta$ -hydroxy amines by enantioselective *N*-oxide formation. *J. Org. Chem.* **1985**, *50*, 4350–4360.
- (27) Kellogg, R. M.; Nieuwenhuijzen, J. W.; Pouwer, K.; Vries, T. R.; Broxterman, Q. B.; Grimbergen, R. F. P.; Kaptein, B.; La Crois, R. M.; de Wever, E.; Zwaagstra, K.; van der Laan, A. C. Dutch resolution: separation of enantiomers with families of resolving agents. A status report. *Synthesis* **2003**, 1626–1638.
- (28) Orjales, A.; Mosquera, R.; Toledo, A.; Pumar, M. C.; Garcia, N.; Cortizo, L.; Labeaga, L.; Innerarity, A. Synthesis and binding studies of new [(aryl)(aryloxy)methyl]piperidine derivatives and related compounds as potential antidepressant drugs with high affinity for serotonin (5-HT) and norepinephrine (NE) transporters. *J. Med. Chem.* **2003**, *46*, 5512–5532.
- (29) Bymaster, F. P.; Beedle, E. E.; Findlay, J.; Gallagher, P. T.; Krushinski, J. H.; Mitchell, S.; Roberston, D. W.; Thomson, D. C.; Wallace, L.; Wong, D. T. Duloxetine (Cymbalta), a dual inhibitor of serotonin and norepinephrine reuptake. *Bioorg. Med. Chem. Lett.* **2003**, *13*, 4477–4480.
- (30) Lee, K.-H.; Park, C.-E.; Min, K.-H.; Shin, Y.-J.; Chung, C.-M.; Kim, H.-H.; Yoon, H.-J.; Won-Kim; Ryu, E.-J.; Shin, Y.-J.; Nam, H.-S.; Cho, J.-W.; Lee, H.-Y. Synthesis and pharmacological evaluation of 3-aryl-3-azolypropan-1-amines as selective triple serotonin/norepinephrine/dopamine reuptake inhibitors. *Bioorg. Med. Chem. Lett.* **2010**, *20*, 5567–5571.
- (31) Williams, J. W.; Morrison, J. F. The kinetics of reversible tight-binding inhibition. *Methods Enzymol.* **1979**, *63*, 437–467.